



1 Fundamental Oxidation Processes in the Remote
2 Marine Atmosphere Investigated Using the NO-
3 NO₂-O₃ Photostationary State
4

5 Simone T. Andersen^{1*}, Beth S. Nelson¹, Katie A. Read^{1,2}, Shalini Punjabi^{1,2}, Luis Neves³,
6 Matthew J. Rowlinson¹, James Hopkins^{1,2}, Tomás Sherwen^{1,2}, Lisa K. Whalley^{2,4}, James D.
7 Lee^{1,2}, and Lucy J. Carpenter¹

8 ¹Wolfson Atmospheric Chemistry Laboratories (WACL), Department of Chemistry,
9 University of York, Heslington, York, YO10 5DD, UK.

10 ²National Centre for Atmospheric Science (NCAS), University of York, Heslington, York,
11 YO10 5DD, UK.

12 ³Instituto Nacional de Meteorologia e Geofísica, São Vicente (INMG), Mindelo, Cabo Verde.

13 ⁴School of Chemistry, University of Leeds, Leeds, LS2 9JT

14 *Corresponding author: simone.andersen@york.ac.uk

15



1 Abstract

The photostationary state (PSS) equilibrium between NO and NO₂ is reached within minutes in the atmosphere and can be described by the PSS parameter, ϕ . Deviations from expected values of ϕ have previously been used to infer missing oxidants in diverse locations, from highly polluted regions to the extremely clean conditions observed in the remote marine boundary layer (MBL), and have been interpreted as missing understanding of fundamental photochemistry. Here, contrary to these previous observations, we observe good agreement between PSS-derived NO₂ ([NO₂]_{PSS ext.}) calculated from photochemical model predictions of peroxy radicals (RO₂ and HO₂) and measured NO, O₃, and j NO₂, and observed NO₂ in extremely clean air containing low levels of CO (< 90 ppbV) and VOCs. However, in clean air containing small amounts of aged pollution (CO > 100 ppbV), we observed higher levels of NO₂ than inferred from the PSS, with [NO₂]_{Obs.}/[NO₂]_{PSS ext.} of 1.12-1.68 (25th-75th percentile) implying 18.5-104 pptV (25th-75th percentile) of missing RO₂ radicals. Potential NO₂ measurement artefacts have to be carefully considered when comparing PSS-derived NO₂ to observed NO₂, but we show that the NO₂ artefact required to explain the deviation would have to be ~ 4 times greater than the maximum calculated from known interferences. If the missing RO₂ radicals have an ozone production efficiency equivalent to that of methyl peroxy radicals (CH₃O₂), then the calculated net ozone production including these additional oxidants is similar to that observed, within estimated uncertainties, once halogen oxide chemistry is accounted for. This implies that peroxy radicals cannot be excluded as the missing oxidant in clean marine air containing aged pollution, and that measured and modelled RO₂ are both significantly underestimated under these conditions.

40

41 2 Introduction

42 Tropospheric NO, NO₂ and O₃ are rapidly interconverted during the day via reactions
43 (1-3), where NO is oxidised by O₃ into NO₂, which is then photolyzed into NO and O(³P),
44 followed by a fast reaction of O(³P) with O₂ to return O₃.





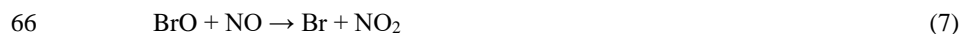
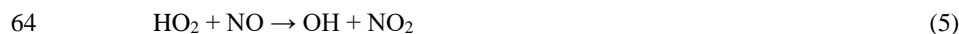
48 The photostationary state (PSS) equilibrium between NO and NO₂ is reached within
49 minutes (Leighton, 1961) if it is not impacted by fresh NO_x emissions and if the photolysis rate
50 does not change quickly such as under rapidly changing cloud coverage (Mannschreck et al.,
51 2004). The photostationary state can be described by the Leighton ratio (Leighton, 1961) (eq.
52 I), where $j\text{NO}_2$ is the photolysis rate of NO₂ and ϕ is the PSS parameter.

53
$$\phi = \frac{j\text{NO}_2[\text{NO}_2]}{k_1[\text{NO}][\text{O}_3]}$$
 (I)

54 Under very polluted conditions, where O₃ is the only oxidant converting NO to NO₂, ϕ
55 is equal to 1 and the NO₂ at PSS can be estimated from the measured NO, O₃, and $j\text{NO}_2$ (eq.
56 II).

57
$$[\text{NO}_2]_{\text{PSS}} = \frac{k_1[\text{NO}][\text{O}_3]}{j\text{NO}_2}$$
 (II)

58 Deviations from $\phi = 1$ suggest the presence of additional chemistry occurring (Calvert
59 and Stockwell, 1983), particularly the conversion of NO to NO₂ by reaction with an oxidant
60 other than O₃, such as hydroperoxy radicals (HO₂) and peroxy radicals (RO₂) (reactions 4-5,
61 where R represents any organic functional group) or with halogen oxides (IO, BrO; reactions
62 6-7) in the marine atmosphere.



67 By including these additional NO oxidation reactions, the NO₂ concentration at PSS
68 can be estimated using equation (III). The photostationary state of NO/NO₂ can also be used to
69 estimate the sum of HO₂ and RO₂ (RO_x) or the sum of BrO and IO (XO) in the atmosphere
70 using equation (IV) and (V) and assuming that $k_4 = k_5$ and $k_6 = k_7$, respectively:

71
$$[\text{NO}_2]_{\text{PSS ext.}} = \frac{(k_1[\text{O}_3] + k_4[\text{RO}_2] + k_5[\text{HO}_2] + k_6[\text{IO}] + k_7[\text{BrO}])([\text{NO}])}{j\text{NO}_2}$$
 (III)



$$72 \quad [\text{RO}_2] + [\text{HO}_2] = \frac{j\text{NO}_2[\text{NO}_2] - (k_1[\text{O}_3] + k_6[\text{IO}] + k_7[\text{BrO}])[\text{NO}]}{k_{4,5}[\text{NO}]} \quad (\text{IV})$$

$$73 \quad [\text{BrO}] + [\text{IO}] = \frac{j\text{NO}_2[\text{NO}_2] - (k_1[\text{O}_3] + k_4[\text{RO}_2] + k_5[\text{HO}_2])[\text{NO}]}{k_{6,7}[\text{NO}]} \quad (\text{V})$$

74 Previous studies reporting deviations in the PSS parameter to estimate RO_x
75 concentrations in the atmosphere are summarised in Table 1, which compares $[\text{RO}_x]_{\text{PSS}}$ against
76 measured and/or modelled $[\text{RO}_x]$. Measurements of RO_x are predominantly conducted using
77 chemical amplification, where each RO_2 and HO_2 molecule in ambient air leads to the
78 formation of several NO_2 molecules by chain reactions caused by the addition of high
79 concentrations of NO and CO (Cantrell et al., 1993b). The resultant NO_2 can be detected and
80 converted back to a RO_x concentration by quantification of the chain length of the reactions
81 via calibration, typically using known concentrations of CH_3O_2 or peroxyacetyl ($\text{CH}_3\text{C}(\text{O})\text{O}_2$)
82 radicals (Cantrell et al., 1993b; Miyazaki et al., 2010; Wood and Charest, 2014). Since the basis
83 of the chemical amplification technique is detection of RO_x radicals from their ability to oxidise
84 NO to NO_2 (reactions 4 and 5), which is also used to estimate RO_x from the PSS, the RO_x
85 concentrations determined from these methods would be expected to agree reasonably well.
86 However, PSS-derived RO_x concentrations are generally higher than both measured and
87 modelled values in rural conditions (Cantrell et al., 1997; Cantrell et al., 1993a; Ma et al., 2017;
88 Mannschreck et al., 2004; Volz-Thomas et al., 2003) with exceptions such as in the Pearl River
89 Delta where PSS-derived and measured RO_x were comparable (Ma et al., 2017). During
90 campaigns in relatively clean regions with moderate influence from pollution (Amazon Basin
91 and Arabian Peninsula), PSS-derived RO_x levels have been shown to be in good agreement
92 with modelled RO_x (Tadic et al., 2020; Trebs et al., 2012). In the remote marine boundary layer
93 (MBL), PSS-derived RO_x has been observed to be 1.27 times higher than the measured RO_x
94 over the South Atlantic Ocean, however, the measured RO_x was approximately 4 times higher
95 than modelled (Hosaynali Beygi et al., 2011).

96 The difference between measured, modelled, and PSS-derived RO_x can be due to a
97 variety of reasons. RO_x concentrations calculated by box models rely on comprehensive
98 constraint from co-measured trace gases and a reaction scheme which accurately represents the
99 most important photochemical processes. Incomplete characterization of ambient trace gases
100 and/or reaction schemes can therefore result in uncertain RO_x predictions. Large deviations
101 (factor of ~ 3) between modelled and measured RO_x levels in a pine forest in the Rocky
102 Mountains were attributed to a combination of a missing photolytic source of HO_2 at midday



103 and a missing reaction forming RO_2 independently of sunlight in the model scheme (Wolfe et
104 al., 2014). PSS-derived RO_x can be significantly over- or underestimated if the PSS has not
105 been established, for example due to rapidly changing photolysis rates or local sources of NO_x
106 (Mannschreck et al., 2004). Another reason for overestimation of PSS-derived RO_x is NO_2
107 measurement artefacts (Bradshaw et al., 1999; Crawford et al., 1996), which results in
108 overestimated NO_2 concentrations. These are common in chemiluminescence instruments and
109 can be due to photolytic or thermal decomposition of HONO, peroxyacetyl nitrate (PAN), and
110 other nitrate molecules in the atmosphere (Bradshaw et al., 1999; Gao et al., 1994; Parrish et
111 al., 1990; Pollack et al., 2010; Reed et al., 2016; Ridley et al., 1988; Ryerson et al., 2000).

112 Measurements of RO_x are also not without challenges due to effects from e.g. the high
113 reactivity of RO_x , humidity, non-linearity of the NO_2 detection, and formation of organic
114 nitrates and nitrites. In the first chemical amplification instruments, NO_2 was detected by
115 luminol chemiluminescence, which has a non-linear response to NO_2 resulting in the need for
116 a multipoint calibration (Cantrell et al., 1997). However, more recent instruments use cavity
117 absorption phase shift (CAPS) (Duncianu et al., 2020; Wood and Charest, 2014), laser induced
118 fluorescence (LIF) (Sadanaga et al., 2004), or cavity ring-down spectroscopy (CRDS) (Liu and
119 Zhang, 2014) for detection of NO_2 , all of which have been shown to have a linear response.
120 Chemical amplifiers are usually only calibrated for one or two types of peroxy radicals.
121 However, the chain length of each peroxy radical varies, resulting in a different amount of NO_2
122 production depending on the mixture of peroxy radicals present, which could lead to
123 over/underestimations depending on the ambient mixture. Additionally, the chain length is
124 significantly affected by humidity due to the increase in HO_2 wall loss on wet surfaces and to
125 an enhanced termination rate of HO_2 by reaction with NO to give HNO_3 . HO_2 has been shown
126 to form a complex with H_2O ($\text{HO}_2\cdot\text{H}_2\text{O}$), which reacts 4-8 times faster with NO , creating
127 HNO_3 , at 50% relative humidity (RH) compared to under dry conditions (Butkovskaya et al.,
128 2007; Butkovskaya et al., 2009; Duncianu et al., 2020). This leads to the measured chain length
129 decreasing by a factor of two when going from dry conditions to 40% RH and by a factor of
130 three at 70% RH (Duncianu et al., 2020; Mihele and Hastie, 1998). Finally, the chain length is
131 impacted by the gas reagents (NO and CO). Peroxy radicals and alkoxy radicals (RO) can react
132 with NO to create organic nitrates and nitrites, which terminates the chain reaction, preventing
133 further radical propagation processes. This is favoured by longer chain peroxy radicals, and at
134 high NO concentrations. The formation yield of organic nitrates and nitrites differs from a few
135 percent to up to ~23% depending on the nature of the R group present (Duncianu et al., 2020).



136 It is therefore important to determine the optimal concentrations of reagent gas for each
137 individual instrument as it could vary with what material has been used in the reactor.

138 In the presence of sufficient levels of NO, additional ambient peroxy radicals not
139 accounted for in photochemical models should lead to an underestimation of the simulated
140 production rate of O₃, which occurs via reactions (4) and (5) followed by photolysis of NO₂.
141 The production of O₃ (P(O₃)) can be calculated using equation (VI):

$$142 \quad P(\text{O}_3) = k_4[\text{NO}][\text{RO}_2] + k_5[\text{NO}][\text{HO}_2] \quad (\text{VI})$$

143 Volz-Thomas et al. (2003) calculated O₃ production rates from PSS-derived and
144 chemical amplification-measured RO_x during the BERLIOZ campaign in Pabstthum,
145 Germany, resulting in an average of ~ 20 ppbV h⁻¹ and ~ 2 ppbV h⁻¹ across the campaign,
146 respectively. The large difference was credited to an unknown process that converts NO into
147 NO₂ without causing additional O₃ production (Volz-Thomas et al., 2003). This is possible if
148 NO is oxidised by an oxidant which also destroys O₃, similarly to halogen atoms/halogen
149 oxides. This hypothesis is consistent with observations by Parrish et al. at a mountain station
150 in Colorado, where a missing oxidant of photolytic origin was identified (Parrish et al., 1986).
151 It was shown that if the NO to NO₂ oxidation was completely due to RO_x, the increased O₃
152 production would result in O₃ mixing ratios significantly higher than measured, yet if the
153 oxidant exhibited similar reaction mechanisms to IO, extremely high (70 pptV) mixing ratios
154 of IO would be needed (Parrish et al., 1986). These IO levels are more than an order of
155 magnitude higher than observations in the marine atmosphere (Inamdar et al., 2020; Mahajan
156 et al., 2010; Prados-Roman et al., 2015; Read et al., 2008).

157 In regions where the net O₃ production is negligible or negative during the day due to
158 very low NO levels, it is more relevant to compare the net ozone production rate (NOPR) to
159 the observed change in O₃. The chemical NOPR can be calculated as the difference between
160 the photochemical processes producing and destroying O₃:

$$161 \quad \text{NOPR} = P(\text{O}_3) - L(\text{O}_3) \quad (\text{VII})$$

162 where P(O₃) is determined using equation (VI) and the loss rate of O₃ (L(O₃)), is usually
163 determined from reactions (8-12). Additionally, halogens have previously been shown to cause
164 an O₃ loss of 0.23 ± 0.05 ppbV h⁻¹ in the MBL (initiated by reaction 13) (Read et al., 2008),
165 which is in line with other studies suggesting that halogens can have a significant impact on O₃
166 in marine environments (Saiz-Lopez et al., 2012; Sherwen et al., 2016; Vogt et al., 1999).



173 The actual rate of change of O_3 within the planetary boundary layer is also impacted by
174 the physical processes of advection, deposition and entrainment, which complicates
175 comparisons with the NOPR. However, if these physical processes change only negligibly over
176 the course of a day, such as in marine well mixed air masses, their net influence can be deduced
177 from the net night time change in O_3 (Ayers and Galbally, 1995; Ayers et al., 1992; Read et
178 al., 2008), allowing a calculation of the NOPR from observations. A comparison of the
179 observed and calculated NOPR gives an indication of whether production and loss rates of O_3
180 from known processes are sufficient to explain the photochemical regime (Read et al., 2008).

181 From the studies shown in Table 1, there is clearly widespread evidence of enhanced
182 PSS-derived RO_2 compared to measurements and models, however, all methods to derive RO_x
183 are not without challenges as described above. The large uncertainties associated with RO_x
184 measurements, especially at high humidities where the chain length is significantly impacted
185 by enhanced wall loss and the production of HNO_3 , suggest that measurements could be
186 underestimating RO_x in the atmosphere. Previous studies also find that the additional
187 conversion of NO to NO_2 caused by the extra “ RO_2 ” should only produce minimal additional
188 O_3 , or at least lead to additional O_3 destruction, thus inferring an unknown missing oxidant
189 which exhibits different chemical behaviour to peroxy radicals.

190 Up to 25% of methane removal occurs in the tropical MBL due to the high
191 photochemical activity and humidity resulting in high OH radical concentrations (Bloss et al.,
192 2005). Thus, it is crucially important to understand the fundamental oxidation processes, such
193 as the NO_x - O_3 cycle, occurring in this region. However, remote NO_x measurements are rare
194 due to the difficulty in measuring very low (pptV) mixing ratios. Most previous remote NO_x
195 measurements have taken place during short campaigns and do not give information on
196 seasonal changes and long-term trends (Carsey et al., 1997; Jacob et al., 1996; Peterson and



197 Honrath, 1999; Rhoads et al., 1997). Here, we investigate the photostationary state under clean
198 marine conditions from three years of observations (2017-2020) at the Cape Verde
199 Atmospheric Observatory (CVAO) in the tropical east Atlantic, representing a unique dataset
200 to investigate NO_x-O₃ chemistry in the remote MBL (Andersen et al., 2021; Carpenter et al.,
201 2010; Lee et al., 2009). We also compare the chemical net O₃ production rate (NOPR)
202 calculated from a box model with NOPR derived from the observed net O₃ rate of change, in
203 order to evaluate the possibility of missing peroxy radicals in this remote environment.

204

205 3 Methods

206 3.1 Measurements

207 Year-round measurements of meteorological parameters and trace gases including NO,
208 NO₂, and C₂-C₈ VOCs have been conducted at the CVAO (16° 51' N, 24° 52' W) since October
209 2006. The CVAO is located on the north eastern coast of São Vicente, Cabo Verde. The air
210 sampled predominantly comes from the northeast (see Figure 1) and has travelled over the
211 Atlantic Ocean for multiple days since the last exposure to anthropogenic emissions, with the
212 potential exception of ship emissions (Carpenter et al., 2010; Read et al., 2008). This makes it
213 an ideal location to investigate fundamental photochemistry in an ultra-clean environment.

214 Wind speed (m/s), wind direction (°), temperature (°C), relative humidity (%),
215 barometric pressure (mbar) and total solar radiation (W/m²) are measured at a height of 7.5 m
216 using an automatic weather station from Campbell Scientific. NO and NO₂ have been measured
217 using an ultra-high sensitivity NO chemiluminescence instrument, which measures NO₂ by
218 photolytic conversion to NO, at the CVAO since 2006 (Lee et al., 2009). The technique and
219 data analysis have been described in detail elsewhere (Andersen et al., 2021). O₃ is measured
220 using a Thermo Scientific 49i Ozone monitor as described in Read et al. (2008). Photolysis
221 rates of a variety of species were measured in 2020 using a spectral radiometer (a 2-pi sr quartz
222 diffuser coupled to an Ocean Optics QE65000 spectrometer via a 10 m fibre optic cable). Prior
223 to 2020, photolysis rates are calculated in this study based on the correlation between the
224 measured photolysis rates in 2020 and the total solar radiation, as described in the
225 supplementary information. Average j_{NO_2} and $j_{\text{O}(^1\text{D})}$ for different seasons are shown in Table
226 2. VOCs are measured using a dual channel Agilent 7890A gas chromatograph coupled with a
227 Flame Ionization Detector (GC-FID) and a MARKES Thermal Desorption Unit with an ozone



228 precursor trap that is cooled to $-30\text{ }^{\circ}\text{C}$ (Read et al., 2009). Details of the calibration and
229 uncertainties are given in the World Calibration Centre (WCC)-VOC audit report
230 (Steinbrecher, 2019). Examples of the VOCs measured at the CVAO can be found in Table 2.
231 Carbon monoxide (CO), and methane (CH_4), are measured using a cavity ring-down
232 spectrometer (CRDS), G2401 manufactured by Picarro Inc, following the Global Atmosphere
233 Watch (GAW) recommended technique for long term remote measurements. The instrument
234 is highly linear, has a precision of 1 ppbV and 0.3 ppbV over 10 minutes for CO and CH_4
235 respectively and no measurable drift (Zellweger et al., 2016; Zellweger et al., 2012).

236 Time series of NO, NO_2 , O_3 , $j\text{NO}_2$, $j\text{O}(^1\text{D})$, temperature, CO, propene, benzene and
237 CH_4 for July 2017 – June 2020 are shown in figures S4-S6. The specifics of each instrument
238 and their respective measurements can be found in Table 2 and a full description of the CVAO
239 site and associated measurements is given in Carpenter et al. (2010).

240

241 3.1.1 NO_2 Measurement Artefact

242 One of the drawbacks of measuring NO_2 by photolytic conversion to NO is it can be
243 subject to artefacts. These could either be of a photolytic or thermal origin (Bradshaw et al.,
244 1999; Gao et al., 1994; Parrish et al., 1990; Ridley et al., 1988; Ryerson et al., 2000). Photolytic
245 artefacts occur when other compounds containing -NO, $-\text{NO}_2$, or $-\text{NO}_3$ photolyse to form NO
246 over a similar wavelength range as NO_2 and thereby produce an overestimate of NO_2 in the
247 sample (Pollack et al., 2010). Thermal artefacts are caused by thermally labile compounds
248 which decompose in photolytic converters when they heat up and release NO that is measured
249 by the detector or NO_2 which is immediately photolytically converted to NO and then detected
250 (Reed et al., 2016). The maximum potential NO_2 artefact can be estimated using measured or
251 modelled mixing ratios of a range of potential interfering compounds. The photolytic
252 contribution can be estimated based on the absorption cross section (ACS) of NO_2 and the
253 potential interferents around the peak wavelength of the diodes used to convert NO_2 into NO
254 (385 nm). The ACS of NO_2 and some known interfering compounds over the wavelength range
255 380-390 nm are shown in Table 3. NO_2 and most of the interferents, with the exception of
256 HONO, show relatively invariant ACSs across these wavelengths. When the ACSs of both NO_2
257 and the particular interferent are invariant over the spectral output of the diodes, the ratio at the
258 peak wavelength is used to estimate the potential artefact. However, since the ACS of HONO
259 varies significantly over the range, the HONO/ NO_2 ACS ratio has been estimated assuming a



260 Gaussian output of the diodes over the wavelengths. It is also important to take into account
261 whether photolysis of the potential interferent produces NO_2 or NO . If NO_2 is the product then
262 it will be photolysed to NO with the same efficiency as NO_2 in the ambient air, however, if NO
263 is the product then 1 converted molecule will be detected as 2 NO_2 molecules if the conversion
264 efficiency of NO_2 is 50 %. Organic nitrates, HNO_3 , and NO_3 do not photolyse at 385 nm and
265 have therefore not been included in the evaluation of photolytic artefacts.

266 The main potential photolytic artefact for the CVAO NO_2 measurements is HONO.
267 Measurements of HONO at the CVAO using a Long Path Absorption Photometer (LOPAP)
268 show levels of up to ~ 5 pptV (Reed et al., 2017), indicating an NO_2 artefact of up to 0.63 pptV.
269 However, these measurements were made using a thermostated inlet system with reactive
270 HONO stripping, where loss of HONO to the sample lines is minimised. The NO_x instrument
271 at the CVAO samples at the end of the manifold making it highly likely that a significant
272 fraction of HONO is lost on the manifold before the air is introduced to the NO_x instrument
273 due to the high surface reactivity of HONO (Pinto et al., 2014). Thus, we regard the potential
274 HONO-induced artefact of 0.63 pptV as an upper limit. No other potential photolytic artefacts
275 have been measured at the CVAO, however using the GEOS-Chem model (see section 3.2.2)
276 we calculated seasonal cycles of 20 potential interfering compounds at the CVAO (Figure S7).
277 None of these compounds exhibit major seasonal differences, indicating that any measurement
278 artefact will be fairly constant across the year. The contribution from photolytic degradation of
279 compounds other than HONO is predicted to be less than 0.05 pptV using the estimated
280 conversion efficiency of each compound in Table 3 and the modelled mixing ratios at the
281 CVAO.

282 Peroxyacetyl nitrate (PAN) is produced in polluted areas and transported to remote
283 regions, where it can thermally decompose into peroxy radicals and NO_2 . 5.8% of the available
284 PAN has been shown to thermally decompose in blue light converters (BLC) switched on 40%
285 of the time (Reed et al., 2016). This can cause significant overestimations of NO_2 in colder
286 regions where PAN can build up in the atmosphere due to its long lifetime (Kleindienst, 1994),
287 however, in warmer regions such as Cabo Verde the overestimation will be substantially lower
288 due to the much shorter lifetime (~ 40 -230 minutes at 25°C) (Bridier et al., 1991; Kleindienst,
289 1994), and hence lower concentration of PAN. At the CVAO, PAN has been measured in
290 February 2020 using gas chromatography as described by Whalley et al. (Whalley et al., 2004),
291 however, all measurements were below the limit of detection (LOD) of 6 pptV. The photolytic
292 converter (PLC) used at the CVAO is only switched on 20% of the time, so a thermal



293 decomposition efficiency of 5% for PAN is used to estimate a potential artefact of 0.3 pptV
294 from PAN. Combining photolytic and thermal artefact contributions gives a maximum
295 potential NO₂ artefact of 0.97 pptV at the CVAO, which is within the uncertainty previously
296 reported for the NO₂ measurements, see Table 2 (Andersen et al., 2021).

297

298 3.2 Modelling

299 3.2.1 Chemical Box Modelling

300 A tailored zero-dimensional chemical box model of the lower atmosphere,
301 incorporating a subset of the Master Chemical Mechanism (MCM v3.3.1) (Jenkin et al., 2015)
302 into the AtChem2 modelling toolkit (Sommariva et al., 2020), was used to estimate
303 concentrations of OH, HO₂ and RO₂ and daily chemical production and loss of O₃ at the CVAO.
304 The MCM describes the detailed atmospheric chemical degradation of 143 VOCs, through
305 17,500 reactions of 6900 species. More details can be found on the MCM website
306 (<http://mcm.york.ac.uk>, last access: 4th March 2022). A fixed deposition rate of $1.2 \times 10^{-5} \text{ s}^{-1}$
307 was applied to all model generated species, giving them a lifetime of approximately 24 hours.
308 The model was constrained to 34 observationally derived photolysis rates, temperature,
309 pressure, and relative humidity, along with a range of observed chemical species, defined in
310 Table 2.

311

312 3.2.2 GEOS-Chem

313 Concentrations of 20 different chemical species were extracted every hour during 2019
314 at nearest point in space and time from the GEOS-Chem model (v12.9.0,
315 DOI:10.5281/zenodo.3950327). The v12.9.0 model as described by Wang et al. (2021) was run
316 at a nested horizontal resolution of 0.25x0.3125 degrees over the region (-32.0 to 15.0 °E, 0.0
317 to 34.0 °N), with boundary conditions provided by a separate global model run spun up for one
318 year and with acid uptake on dust considered as described by Fairlie et al. (2010) (Fairlie et al.,
319 2010; Wang et al., 2021).

320



321 4 Results and Discussion

322 Monthly diurnal cycles of HO₂, RO₂, and OH were modelled by constraining the box
323 model to the measurements described in Table 2 (except NO₂) using hourly median
324 concentrations for each month from July 2017 – June 2020 where all the trace gas
325 measurements were available. When measured $j\text{O}(^1\text{D})$ was not available, the hourly average
326 from the same month across the other years was used. Calculated photolysis rates based on
327 total solar radiation (see supplementary) were used up to December 2019 for all other
328 photolysis rates than $j\text{O}(^1\text{D})$.

329 The modelled OH, HO₂ and RO₂ concentrations agree reasonably well with previous
330 measurements from short term field campaigns based at the CVAO and from various cruises
331 in the Atlantic Ocean (see Figure 2). All the previous measurements of RO_x (HO₂ + RO₂)
332 shown in Figure 2 were conducted using the chemical amplifier technique, which is subject to
333 high uncertainties due to the challenges described above. Daily diurnal cycles of RO₂ and HO₂
334 for 9 days in August 2017, 12 days in October 2017, and 20 days in January 2018 were
335 modelled to investigate their daily variability (see Figure S8). Seasonal differences can be
336 observed from the daily outputs, but no major day to day changes within a given month.

337

338 4.1 Comparison of measured and PSS NO₂ concentrations

339 Daily midday (12.00-15.00 UTC, local+1) NO₂ mixing ratios were calculated from the
340 Leighton ratio using equation II ($[\text{NO}_2]_{\text{PSS}}$), the measured NO, O₃, and $j\text{NO}_2$ and $k_1 = 2.07 \times$
341 $10^{-12} \times e^{(-1400/T)}$ (Atkinson et al., 2004) for a three-year period (July 2017 – June 2020). Figure
342 3A shows that $[\text{NO}_2]_{\text{PSS}}$ significantly underestimates the measured NO₂, indicating that
343 additional oxidants are needed to convert NO into NO₂. Daily midday values of $[\text{NO}_2]_{\text{PSS ext.}}$
344 were calculated using equation III, where a midday average of each modelled monthly diurnal
345 cycle of HO₂ and RO₂ in Figure 2 was used for all days of their respective month together with
346 previous yearly averaged midday measurements of IO (1.4 ± 0.8 pptV) and BrO (2.5 ± 1.1
347 pptV) (Mahajan et al., 2010; Read et al., 2008) at the CVAO. RO₂ was assumed to be equivalent
348 to CH₃O₂, making $k_4 = 2.3 \times 10^{-12} \times e^{(360/T)}$, $k_5 = 3.45 \times 10^{-12} \times e^{(270/T)}$, $k_6 = 7.15 \times 10^{-12} \times e^{(300/T)}$,
349 and $k_7 = 8.7 \times 10^{-12} \times e^{(260/T)}$ (Atkinson et al., 2004). $[\text{NO}_2]_{\text{PSS ext.}}$ was calculated using a midday
350 average of the modelled monthly $[\text{HO}_2]$ and $[\text{RO}_2]$ in Figure 2 as well as the modelled daily
351 midday averages from the diurnal cycles in Figure S8 for August 2017, October 2017, and



352 January 2018. A scatter plot of monthly vs daily calculated $[\text{NO}_2]_{\text{PSS ext.}}$ around the 1:1 line (see
353 Figure S9) verifies the use of monthly calculated $[\text{HO}_2]$ and $[\text{RO}_2]$ for the remaining analyses.

354 Figure 3B shows that the agreement between measured NO_2 and $[\text{NO}_2]_{\text{PSS ext.}}$ was
355 improved significantly by including modelled additional oxidants. At NO_2 mixing ratios below
356 20 pptV, the scatter of $[\text{NO}_2]_{\text{PSS ext.}}$ vs $[\text{NO}_2]_{\text{Obs.}}$ was close to the 1:1 line, however, at higher
357 NO_2 mixing ratios $[\text{NO}_2]_{\text{PSS ext.}}$ under-predicts the observed NO_2 mixing ratio by on average
358 9.5 pptV. NO_2 mixing ratios above 20 pptV are predominantly observed at the CVAO from
359 December-February (Andersen et al., 2021), which coincides with the arrival of predominantly
360 African air to the site (see Figure 1).

361 We next investigate the effects of seasons and the abundance of NO on the ability of
362 the full PSS equation (equation III) to predict NO_2 . Daily midday averages of
363 $[\text{NO}_2]_{\text{Obs.}}/[\text{NO}_2]_{\text{PSS ext.}}$ are plotted as a function of NO in Figure 4. A ratio of 1 would be
364 expected if all relevant reaction mechanisms have been taken into account. The deviations from
365 1 in the ratio can be observed to increase with decreasing NO mixing ratio during March-
366 December. The dashed lines in Figure 4 visualise the effect of a constant NO_2 artefact of 0.97
367 pptV (our calculated upper limit) on the $[\text{NO}_2]_{\text{Obs.}}/[\text{NO}_2]_{\text{PSS ext.}}$ ratio, showing that the artefact,
368 while small, can explain some of this observed trend. However, only a small dependence on
369 the NO mixing ratio is seen for January and February, where enhancements of
370 $[\text{NO}_2]_{\text{Obs.}}/[\text{NO}_2]_{\text{PSS ext.}}$ above 1 continue out to 10 pptV of NO. At Hohenpeissenberg, Germany,
371 similar trends with increasing NO_2/NO ratio with decreasing NO have been observed, which
372 were partly explained by measurement uncertainty in NO and partly by the PSS not being
373 established after being perturbed by NO_x emissions or variable $j\text{NO}_2$ (Mannschreck et al.,
374 2004). An opposite trend to that observed here and at Hohenpeissenberg was observed over the
375 South Atlantic Ocean, with increasing deviations in $[\text{NO}_2]_{\text{Obs.}}/[\text{NO}_2]_{\text{PSS ext.}}$ with increasing NO_2
376 from 3-20 pptV (Hosaynali Beygi et al., 2011), which was explained by a missing photolytic
377 oxidation process.

378

379 4.2 NO_2 Artefact or Missing Oxidant?

380 Deviations between $[\text{NO}_2]_{\text{Obs.}}$ and $[\text{NO}_2]_{\text{PSS ext.}}$ are usually attributed to an unaccounted
381 artefact in the NO_2 measurements or a missing oxidant converting NO into NO_2 (Bradshaw et
382 al., 1999; Carpenter et al., 1998; Crawford et al., 1996; Hauglustaine et al., 1999; Hauglustaine



383 et al., 1996; Hosaynali Beygi et al., 2011; Volz-Thomas et al., 2003). As discussed above, we
384 show that below 5 pptV of ambient NO, our calculated maximum NO₂ artefact of 0.97 pptV
385 starts to have an impact on the $[\text{NO}_2]_{\text{Obs.}}/[\text{NO}_2]_{\text{PSS ext.}}$ ratio, however, it is not enough to explain
386 the enhancements observed, especially in wintertime at the CVAO.

387 The production of RO₂ and HO₂ radicals is dependent on the abundance of their VOC
388 and CO precursors as well as on photochemical activity. To investigate whether the availability
389 of VOCs, CO or sunlight was related to the discrepancy between $[\text{NO}_2]_{\text{Obs.}}$ and $[\text{NO}_2]_{\text{PSS ext.}}$,
390 Figure 4 was replotted by colouring the $[\text{NO}_2]_{\text{Obs.}}/[\text{NO}_2]_{\text{PSS ext.}}$ ratio as a function of the mixing
391 ratio of a particular precursor or $j\text{NO}_2$ (Figure 5). The high deviations in $[\text{NO}_2]_{\text{Obs.}}/[\text{NO}_2]_{\text{PSS ext.}}$
392 at NO > 2.5 pptV can be observed to be associated with higher measured mixing ratios of CO,
393 ethane, and acetylene, and lower midday $j\text{NO}_2$, however, it should be noted that the variation
394 in midday photolysis rates at the CVAO over the year is relatively small. At similar $j\text{NO}_2$ as
395 observed at the CVAO at midday (>0.007 s⁻¹), Hosaynali Beygi et al. observed the largest
396 deviations in $[\text{NO}_2]_{\text{Obs.}}/[\text{NO}_2]_{\text{PSS ext.}}$ (Hosaynali Beygi et al., 2011). For the high enhancements
397 in $[\text{NO}_2]_{\text{Obs.}}/[\text{NO}_2]_{\text{PSS ext.}}$ at NO < 2.5 pptV at the CVAO, the trends are not as clear. The mixing
398 ratios of CO can be observed to remain enhanced, however, high $j\text{NO}_2$ is seen at NO < 2.5
399 pptV while the ethane and acetylene mixing ratios are lower than when NO > 2.5 pptV. It is
400 important to note though that the deviation at very low NO can on most days be explained by
401 the measurement uncertainty in NO (~1.4 pptV). Figure 5 shows that the abundances of ethene
402 and propene, both of which have atmospheric lifetimes of less than 3 days, do not seem to
403 affect the deviation of $[\text{NO}_2]_{\text{Obs.}}/[\text{NO}_2]_{\text{PSS ext.}}$ from 1. Conversely, high abundances of CO,
404 ethane, and acetylene, which all have atmospheric lifetimes above 6 weeks (Atkinson et al.,
405 2006), are observed to be associated with higher $[\text{NO}_2]_{\text{Obs.}}/[\text{NO}_2]_{\text{PSS ext.}}$ ratios. This could
406 indicate that long-range transport of pollutants supplies additional peroxy radicals (or other NO
407 to NO₂ oxidants) at the CVAO, which are not predicted from known sources and
408 photochemistry.

409 To further evaluate the impact of pollution, $[\text{NO}_2]_{\text{Obs.}}/[\text{NO}_2]_{\text{PSS ext.}}$ was separated into
410 three categories based on CO mixing ratios; CO < 90 ppbV, 90 ppbV < CO < 100 ppbV, and
411 CO > 100 ppbV. The deviations of $[\text{NO}_2]_{\text{Obs.}}/[\text{NO}_2]_{\text{PSS ext.}}$ from 1 increase with increasing [CO],
412 with 50th (25th-75th) percentiles of 1.10 (0.82 -1.37) for CO < 90 ppbV, 1.20 (0.97-1.54) for 90
413 ppbV < CO < 100 ppbV, and 1.50 (1.18-1.78) for CO > 100 ppbV. The small deviation from
414 1, which is within the uncertainty of our measurements (see below), for CO < 90 ppbV is strong
415 evidence that fundamental oxidation process in ultra-clean marine air, where the main



416 precursors of RO_2 and HO_2 are CH_4 and CO giving CH_3O_2 and HO_2 , respectively, are well
417 understood.

418 An NO_2 artefact of 0.7 pptV would reduce the ratio of 1.10 to 1.00 in air masses with
419 $\text{CO} < 90$ ppbV. Since the minimum value of the artefact is 0 pptV (if there was no conversion
420 of interferent compounds to NO or NO_2), and our estimated upper limit is 0.97 pptV, we
421 therefore consider it a reasonable assumption that the average NO_2 artefact of our instrument
422 at the CVAO is 0.7 pptV. We make the simple *a priori* assumption that this applies across all
423 measurements during the period of analyses. Such an artefact is insignificant when considering
424 total NO_x concentrations, however, it has a non-negligible impact when investigating NO_2/NO
425 ratios in this very low NO_x environment.

426 Subtracting 0.7 pptV from all the NO_2 observations results in median (25th-75th
427 percentiles) ratios of 1.00 (0.76-1.29) for $\text{CO} < 90$ ppbV, 1.14 (0.89-1.47) for $90 \text{ ppbV} < \text{CO}$
428 < 100 ppbV, and 1.42 (1.12-1.68) for $\text{CO} > 100$ ppbV (Table 4). Distributions of each category
429 are plotted in Figure 6A. When CO is between 90 and 100 ppbV, the distribution of
430 $[\text{NO}_2]_{\text{Obs.}}/[\text{NO}_2]_{\text{PSS ext.}}$ shows the highest occurrences at ratios of ~ 1 and ~ 1.5 . When $\text{CO} > 100$
431 ppbV, it is evident that either additional oxidants are needed to convert NO to NO_2 , or an
432 additional NO_2 artefact of the order of 4.4 pptV is present in these air masses. As an artefact of
433 0.7 pptV has already been subtracted, and measurements of HONO and PAN and modelled
434 mixing ratios of halogen nitrates indicate a fairly stable artefact across the year, 4.4 pptV of
435 additional artefact seems highly unlikely. This leaves the possibility of a missing oxidant when
436 the sampled air is enhanced in CO .

437 Using equation (IV) and (V), the required RO_x ($\text{RO}_2 + \text{HO}_2$) and XO ($\text{IO} + \text{BrO}$)
438 concentrations needed to reconcile $[\text{NO}_2]_{\text{Obs.}}$ with $[\text{NO}_2]_{\text{PSS ext.}}$ can be estimated using $k_{4,5} = 2.3$
439 $\times 10^{-12} \times e^{(360/T)}$ and $k_{6,7} = 8.7 \times 10^{-12} \times e^{(260/T)}$ (Atkinson et al., 2004). Our calculations are based
440 on two scenarios: (1) that the measured $[\text{BrO}]$ and $[\text{IO}]$ are correct and there is missing RO_x ,
441 or (2) that the modelled $[\text{RO}_x]$ is correct and there is missing $[\text{XO}]$. Due to the similar rate
442 coefficients for IO and BrO reacting with NO , a combined XO can be estimated. The results
443 are summarised in Table 4 based on the three CO categories. The median required RO_x was
444 determined to be 65.0 (33.68 - 112.5, 25th-75th percentile) pptV and 109.7 (63.14 - 149.5, 25th-
445 75th percentile) pptV for $90 \text{ ppbV} < \text{CO} < 100 \text{ ppbV}$ and $\text{CO} > 100 \text{ ppbV}$, respectively. RO_x
446 measurements during the ALBATROSS cruise varied from 40-80 pptV while in the North
447 Atlantic, however, with a reported uncertainty of 25% (1σ) they could be as high as 100 pptV



448 (Burkert et al., 2001). Such concentrations are comparable to the required median RO_x in this
449 study of 109.7 pptV when $CO > 100$ ppbV. The uncertainty reported for ALBATROSS is
450 similar to many other studies which have reported 10-36% uncertainty on chemical
451 amplification RO_x measurements (Cantrell et al., 1997; Clemitshaw et al., 1997; Handisides et
452 al., 2003; Hernández et al., 2001; Hosaynali Beygi et al., 2011; Volz-Thomas et al., 2003),
453 however, a recent study in the Pearl River Delta reported an uncertainty of 60% (1σ) (Ma et
454 al., 2017). This combined with measurements up to ~ 150 pptV of RO_x in the South Atlantic
455 Ocean (Hosaynali Beygi et al., 2011) indicates that our required RO_x levels of ~ 100 pptV may
456 not be unrealistic in the MBL.

457 The median required RO_x ($[RO_x]_{PSS}$) can be observed to be ~ 2.5 times higher than those
458 modelled for air masses where $CO > 100$ ppbV, whereas the required $[XO]$ is a factor of ~ 6.5
459 higher than previous observations at the CVAO (Mahajan et al., 2010; Read et al., 2008) due
460 to the lower rate coefficients for halogen oxides with NO. Across the three categories, the daily
461 median ratio of $[RO_x]_{PSS}/[RO_x]_{Model}$ is 1.5, which is similar to those observed in previous
462 studies both in remote and rural regions (see Table 1). The missing XO required to reconcile
463 $[NO_2]_{Obs.}$ with $[NO_2]_{PSS ext.}$ was determined for each CO category by subtracting the previous
464 measured average concentration of 3.9 pptV (2.5 pptV BrO + 1.4 pptV IO) from the required
465 XO. Since CO, the main precursor for HO_2 , is constrained by measurements in the model, the
466 calculated $[HO_2]$ is assumed to be correct. Thus, we estimate the required and missing RO_2
467 assuming it is all in the form of CH_3O_2 from:

$$468 \quad [RO_2]_{Required} = \frac{jNO_2[NO_2] - (k_1[O_3] + k_5[HO_2] + k_6[IO] + k_7[BrO])[NO]}{k_4[NO]} \quad (VIII)$$

$$469 \quad [RO_2]_{Missing} = \frac{jNO_2[NO_2] - (k_1[O_3] + k_5[HO_2] + k_6[IO] + k_7[BrO])[NO]}{k_4[NO]} - [RO_2]_{model} \quad (IX)$$

470 Figures 6B and C, show that the missing RO_2 or XO level increases with increasing
471 $[CO]$, reaching a median of 61.3 pptV and 22.7 pptV, respectively, for air masses where $CO >$
472 100 ppbV, which is approximately 2.2 times the modelled RO_2 and 5.5 times the measured XO
473 in the same air masses. Such an increase in peroxy radicals would, under more polluted
474 conditions, cause a major increase in O_3 production during a day (Volz-Thomas et al., 2003).
475 We next examine the impact of missing RO_2 on net O_3 production in Cabo Verde.

476



477 4.3 Chemical O₃ Loss

478 The daily chemical loss of O₃ between 09.30 (09.00-10.00) and 17.30 (17.00-18.00)
479 UTC was used to evaluate whether the PSS-derived [RO₂] was consistent with the net chemical
480 destruction of O₃ at the CVAO. As discussed above, the measured O₃ mixing ratio in the MBL
481 is affected by loss mechanisms in the form of photolysis, reactions with HO_x and halogens, and
482 deposition, and by production through NO₂ photolysis and by entrainment from the O₃-
483 enriched free troposphere. Due to the very stable meteorological condition of the MBL, the
484 variability in entrainment and deposition between night and day is expected to be negligible
485 (Ayers and Galbally, 1995; Ayers et al., 1992; Read et al., 2008). A combined
486 entrainment/deposition term can therefore be estimated from night time O₃ measurements,
487 when there is no photochemical production or loss. An hourly entrainment/deposition term was
488 determined for each month using the average change in O₃ between 22.30 (22.00-23.00) and
489 03.30 (03.00-04.00), and found to vary from 0.18 ppbV h⁻¹ in January to 0.35 ppbV h⁻¹ in May,
490 which is in good agreement with previous measurements at the CVAO of 0.18-0.48 ppbV h⁻¹
491 (Read et al., 2008). The observed daily change in O₃ ($\Delta O_{3 \text{ obs.}}$) (09.30-17.30) was determined
492 to be -0.40 ± 0.32 ppbV h⁻¹ (1 σ) across the three years (2017-2020), which is almost identical
493 to the -0.41 ± 0.33 ppbV h⁻¹ (1 σ) observed at the CVAO in 2007 (Read et al., 2008), but roughly
494 2 times the daily $\Delta O_{3 \text{ obs.}}$ in baseline air at Cape Grim (-0.24 ± 0.32 ppbV h⁻¹, 1 σ) and Mace
495 Head (-0.20 ± 0.21 ppbV h⁻¹, 1 σ) (Carpenter et al., 1997) and 2-40 times the modelled O₃ loss
496 at Mauna Loa (-0.01 to -0.21 ppbV h⁻¹) (Cantrell et al., 1996; Ridley et al., 1992).

497 By subtracting the monthly average entrainment/deposition term from the observed
498 daily ΔO_3 , the daily chemical loss of O₃, $\Delta O_{3 \text{ chem.}}$, is obtained. The observations were filtered
499 to exclude periods where the change in CO concentration over the interval period, ΔCO , was
500 outside 1 standard deviation of the mean ΔCO , to avoid the ΔO_3 determination being affected
501 by changing air masses. The resulting observed chemical loss of O₃ is averaged by month and
502 plotted in black in Figure 7. $\Delta O_{3 \text{ chem.}}$ can be observed to follow photochemical activity, with
503 the lowest $\Delta O_{3 \text{ chem.}}$ in October-February, where the lowest photolysis rates are measured (see
504 supplementary and Table 2) and highest $\Delta O_{3 \text{ chem.}}$ in March-May and September. A small
505 decrease in $\Delta O_{3 \text{ chem.}}$ in June-August occurred simultaneously to the small drop in photolysis
506 rates in June-August. Overall, $\Delta O_{3 \text{ chem.}}$ varied from -0.48 ppbV h⁻¹ in January to -0.88 ppbV h⁻¹
507 in May.



508 In order to evaluate whether these observationally-derived chemical loss rates of O₃ are
509 consistent with PSS-derived peroxy radical concentrations, ΔO_3 chem. was estimated using a
510 chemical box model incorporating the MCM, as described in section 3.2.1. The model was
511 constrained to all the measurements described in Table 2, except NO₂ and O₃, which were left
512 unconstrained. ΔO_3 chem. was simulated with modelled [RO₂] and [HO₂], with (blue line in
513 Figure 7) and without (grey in Figure 7) inclusion of the halogen chemistry described in Table
514 S1, allowing an evaluation of the O₃ loss due to halogens, as previously discussed by Read et
515 al. (2008). Simulations were also performed with [CH₃O₂] constrained to the required RO₂,
516 modelled [HO₂] and including halogen chemistry (orange in Figure 7). In model runs with
517 halogen chemistry, BrO and IO were constrained to previously measured annual averages \pm
518 reported uncertainties (blue shaded area in Figure 7) (Read et al., 2008). Diurnal cycles of the
519 required RO₂ were constructed using the median of the daily midday averages for each month
520 determined using equation (VIII) for the peak concentration at midday, 1 pptV overnight and
521 interpolating linearly in between.

522 Figure 7 shows that all three modelled ΔO_3 chem. exhibited very similar seasonality as
523 the observed ΔO_3 chem.. The difference between running the model with and without halogen
524 chemistry was 0.24 ± 0.02 ppbV h⁻¹ (1 σ), which is almost equivalent to the results of Read et
525 al. (2008) from the CVAO of 0.23 ± 0.05 ppbV h⁻¹ (1 σ). From May-December, the modelled
526 ΔO_3 chem. was almost identical whether using modelled RO₂ or constraining CH₃O₂ to the
527 required RO₂, and both were very similar to observed ΔO_3 chem.. The largest difference in ΔO_3
528 chem. between using modelled RO₂ and constraining CH₃O₂ is observed in January where the
529 difference reached 0.09 ppbV h⁻¹, however, this is caused by constraining CH₃O₂ to 100 pptV,
530 which is 5 times more than the modelled RO₂. The average difference between the observed
531 and modelled ΔO_3 chem. is 0.06 ± 0.07 ppbV h⁻¹ (1 σ) when constraining CH₃O₂ to the required
532 RO₂ and 0.04 ± 0.07 ppbV h⁻¹ (1 σ) when using modelled RO₂.

533 Overall, the very small differences in modelled ΔO_3 chem. whether including the
534 “missing RO₂” or not are a function of the NO_x-limited conditions of the remote MBL, where
535 O₃ production is relatively insensitive to the mixture and abundance of peroxy radicals
536 (Sillman, 1999). Thus, although our analysis shows that peroxy radicals with the equivalent
537 O₃ production potential as CH₃O₂ cannot be ruled out as the missing oxidant in marine air
538 masses with aged pollution, neither does it provide robust evidence that the missing oxidant is
539 O₃-producing. Nevertheless, the deviation between PSS-derived peroxy radicals in this study



540 and previous measurements can potentially be explained by the difficulty in measuring peroxy
541 radicals, as discussed above.

542

543 5 Conclusions

544 In the remote MBL ($\text{CO} < 90$ ppbV, $\text{NO}_x < 43$ pptV (90th percentile = 23 pptV)) we
545 have shown that the observed NO_2/NO ratio is consistent with fundamental photochemical
546 theory, and that neither missing oxidants nor deviations of the photostationary state are required
547 to reconcile observations with the calculated NO_2/NO ratio. This is to our knowledge the first
548 time this has been shown in a low NO_x environment. However, observed NO_2 levels became
549 increasingly higher than predicted as the CO mixing ratio increased and the air more influenced
550 by long range transport of air pollution in winter. A detailed analysis of potential NO_2
551 measurement artefacts at the CVAO showed that such artefacts were unlikely to account for
552 these deviations, thus we evaluated the case for a missing NO to NO_2 oxidant. The required
553 oxidant in air masses with $\text{CO} > 100$ ppbV reached a median of 109.7 pptV when treated as
554 CH_3O_2 . These levels are ~ 2.5 times higher than both our modelled RO_x ($\text{RO}_2 + \text{HO}_2$) and
555 previous measurements of RO_x measured by chemical amplification at the CVAO. However,
556 chemical amplification measurements are known to be highly uncertain due to the difficulty in
557 determining the chain length of the mixture of RO_2 in the ambient matrix, and we note that the
558 modelled O_3 production at the CVAO, with the inclusion of these additional peroxy radicals,
559 did not deviate significantly from the observed O_3 production. Overall, we conclude that there
560 is strong evidence for a missing oxidant in remote marine air impacted by long range transport
561 of pollution, and that peroxy radicals cannot be ruled out as to their identity.

562

563 6 Acknowledgements

564 The authors would like to thank the UK Natural Environment Research Council/
565 National Centre for Atmospheric Science (NERC/NCAS) through the Atmospheric
566 Measurement and Observation Facility (AMOF) for funding the CVAO programme. STA's
567 PhD was supported by the SPHERES Natural Environment Research Council (NERC)
568 Doctoral Training Partnership (DTP), under grant NE/L002574/1. LJC acknowledges funding



569 from the European Research Council (ERC) under the European Union's Horizon 2020 pro-
570 gramme (project O3-SML; grant agreement no. 833290).

571

572 7 Author Contributions

573 Data analysis has been performed by STA. The box model has been run by BSN. Back
574 trajectories have been modelled by MR. GEOS-Chem has been run by TS. The instruments at
575 the CVAO have been run by STA, KAR, SP, JH, and LN. KAR and LKW have processed the
576 spectral radiometer data. The manuscript has been written by STA, LJC, JDL, BSN, and KAR.

577

578 8 Additional Information

579 The authors declare that they have no competing interests.

580

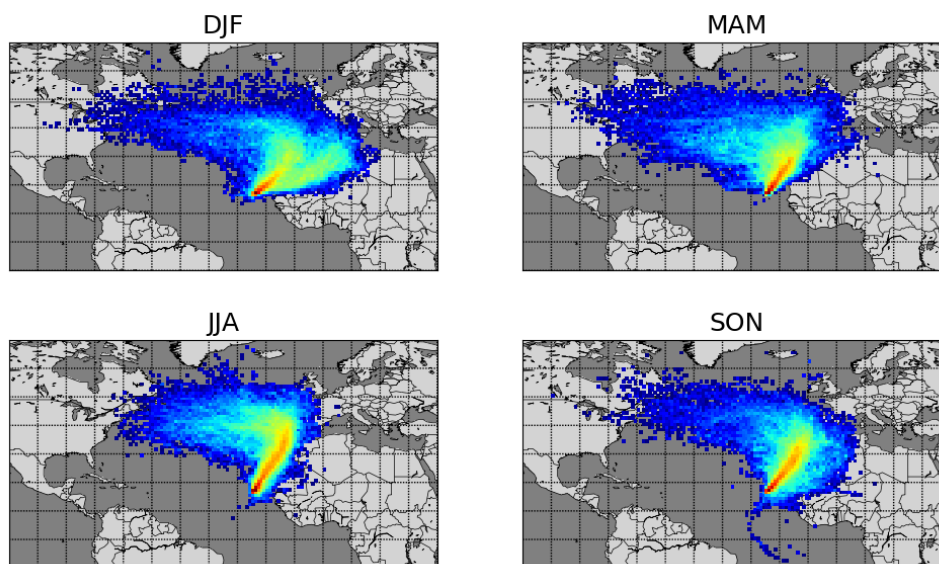
581 8.1 Data availability:

582 NO_x, VOCs, meteorological data, CO and O₃: WDCRG (World Data Centre for
583 Reactive Gases)/Norwegian Institute for Air Research (NILU) EBAS database ([EBAS](https://ebas.nilu.no)
584 [nilu.no](https://ebas.nilu.no))

585 CH₄ and CO: [WDCGG \(World Data Centre for Greenhouse Gases\) \(kishou.go.jp\)](https://wdcgg.kishou.go.jp)

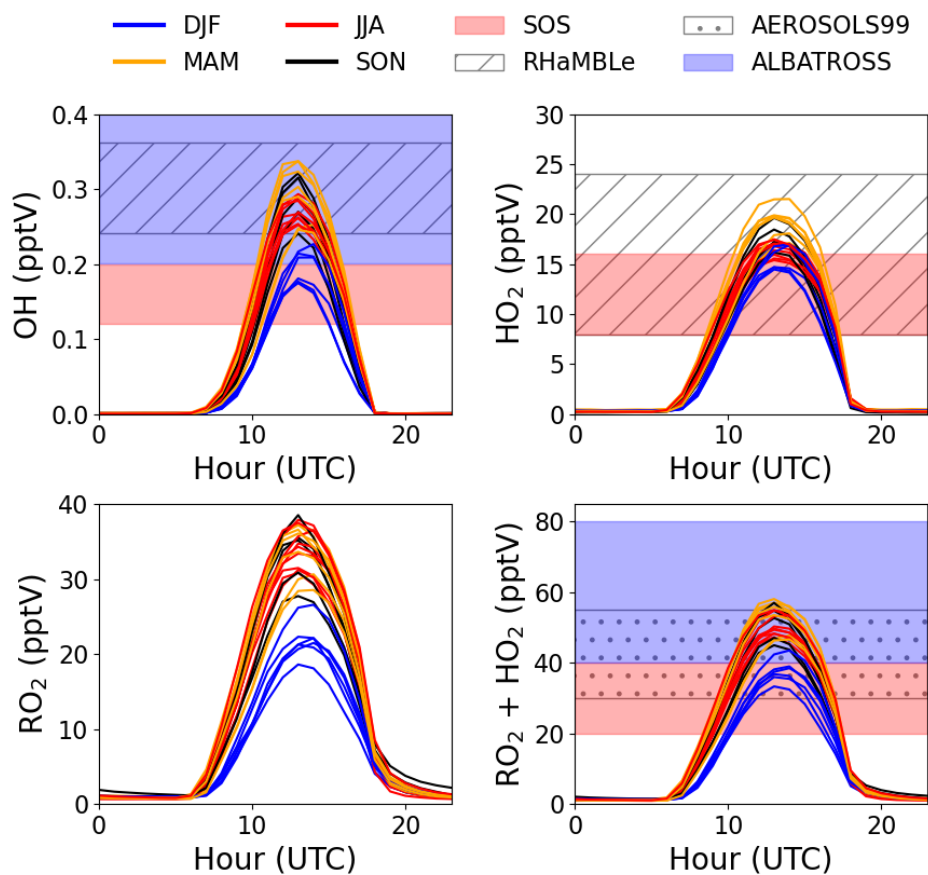


586 9 Figures



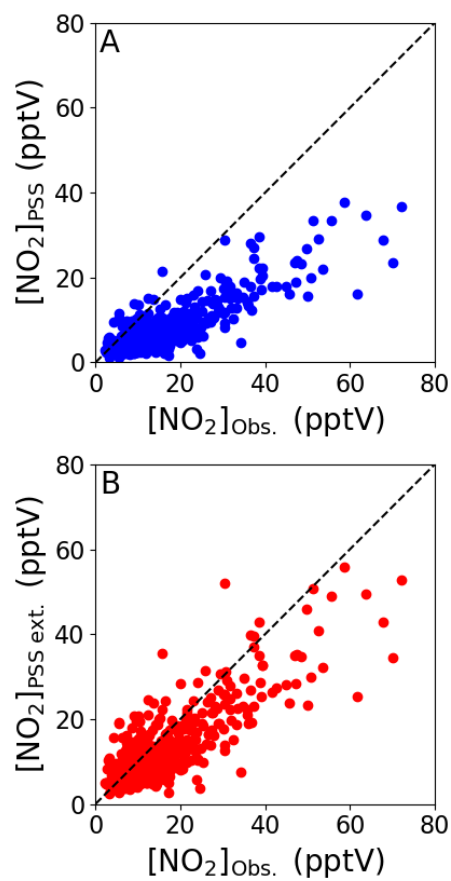
587

588 Figure 1: Seasonal average 10-day back trajectories for the CVAO determined using
589 FLEXPART as described in Andersen et al. (2021).



590

591 Figure 2: Average monthly diurnal cycles of modelled OH, HO₂, RO₂, and HO₂+RO₂ coloured
592 by season compared to midday measurements during SOS (Carpenter et al., 2010; Vaughan et
593 al., 2012), RHaMBLe (Whalley et al., 2010), AEROSOLS99 (Hernández et al., 2001), and
594 ALBATROSS (Burkert et al., 2001).



595

Figure 3: Midday (12.00-15.00 UTC, local+1) daily averages of [NO₂]_{PSS} (A) and [NO₂]_{PSS ext.} (B) plotted against the observed NO₂ using measurements from July 2017 – June 2020. The black dashed lines show the 1:1 ratio.

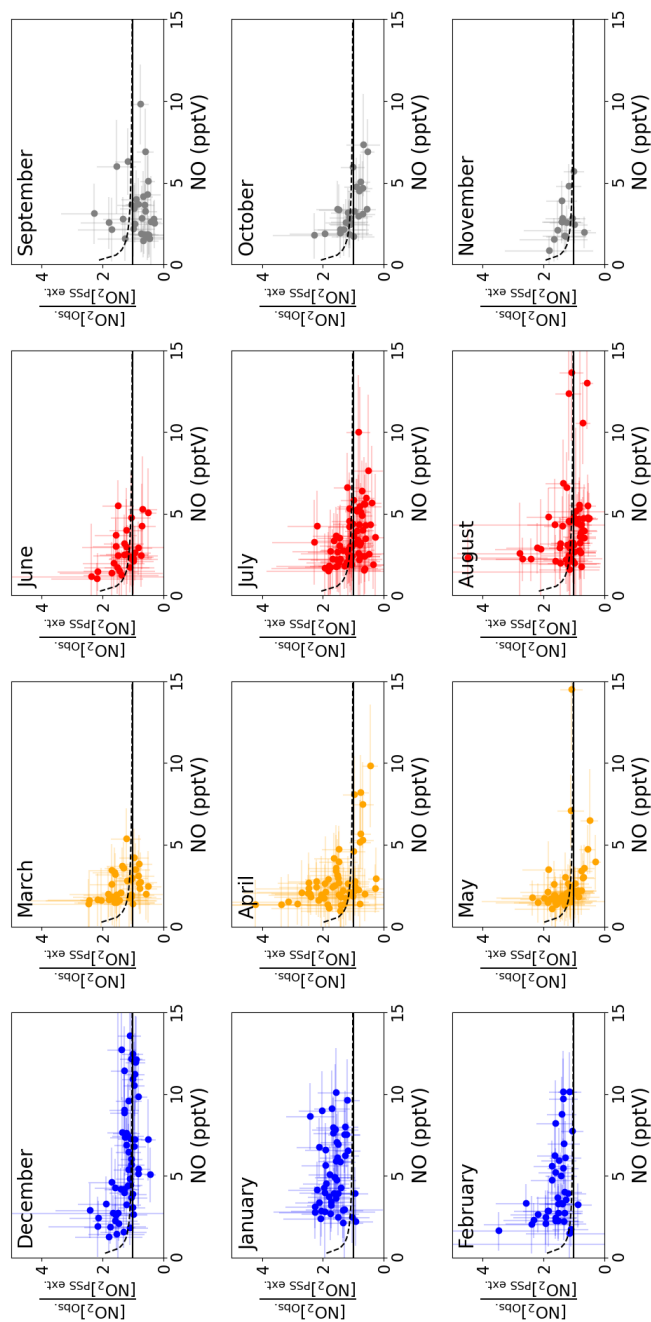
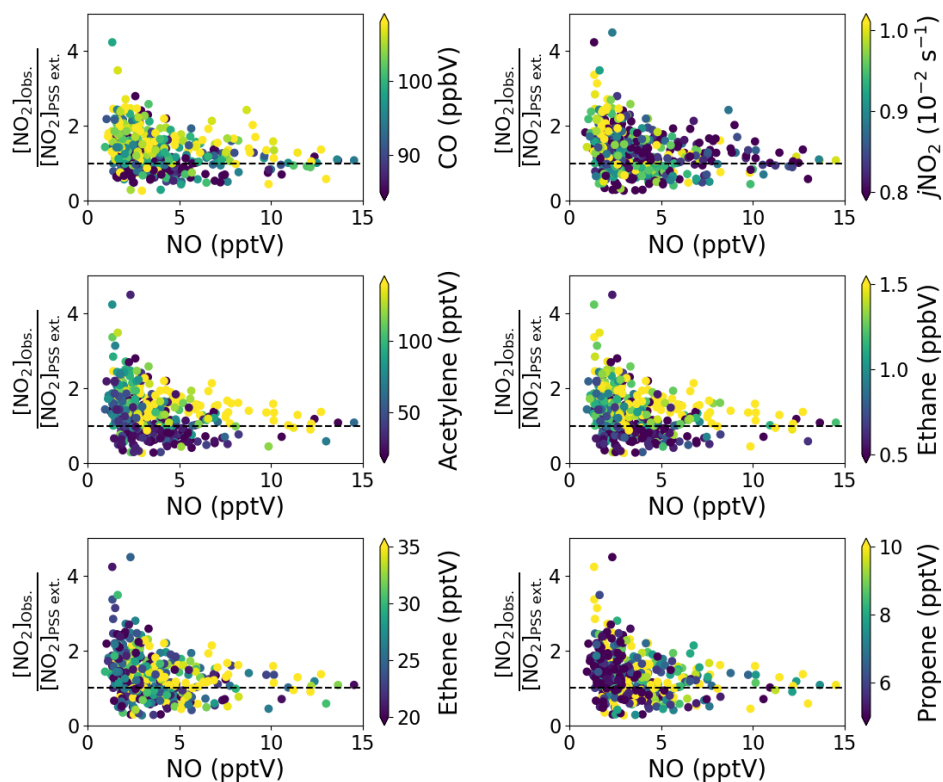


Figure 4: Monthly plots of midday (12.00–15.00 UTC, local+1) daily averages of $[\text{NO}_2]_{\text{obs.}}/[\text{NO}_2]_{\text{PSS ext.}}$ vs. the measured NO mixing ratio. The solid lines represent a ratio of 1 between the observed and predicted NO_2 . The dashed lines represent $([\text{NO}_2]_{\text{PSS ext.}} + 0.97 \text{ pptV})/[\text{NO}_2]_{\text{PSS ext.}}$ to visualise the effect of a NO_2 artefact of 0.97 pptV on measured NO. The data points represent the average measured NO_2 and modelled HO_2 and RO_2 for each month and the annually average measured IO and BrO for the CVAO. The uncertainty of each data point has been determined from measurement uncertainties in Table 2, the uncertainties in the measured BrO and IO described in the text, and 20% uncertainty on all the rate coefficients. The uncertainty in the modelled radicals has not been included



600



601

602 Figure 5: Midday (12.00-15.00 UTC, local +1) daily averages of $[\text{NO}_2]_{\text{Obs.}}/[\text{NO}_2]_{\text{PSS ext.}}$ from
603 July 2017 to June 2020 plotted against the measured NO and coloured by five different
604 measured precursors for either HO₂ or RO₂ and $j\text{NO}_2$. The dashed line represent a ratio of 1

605



606

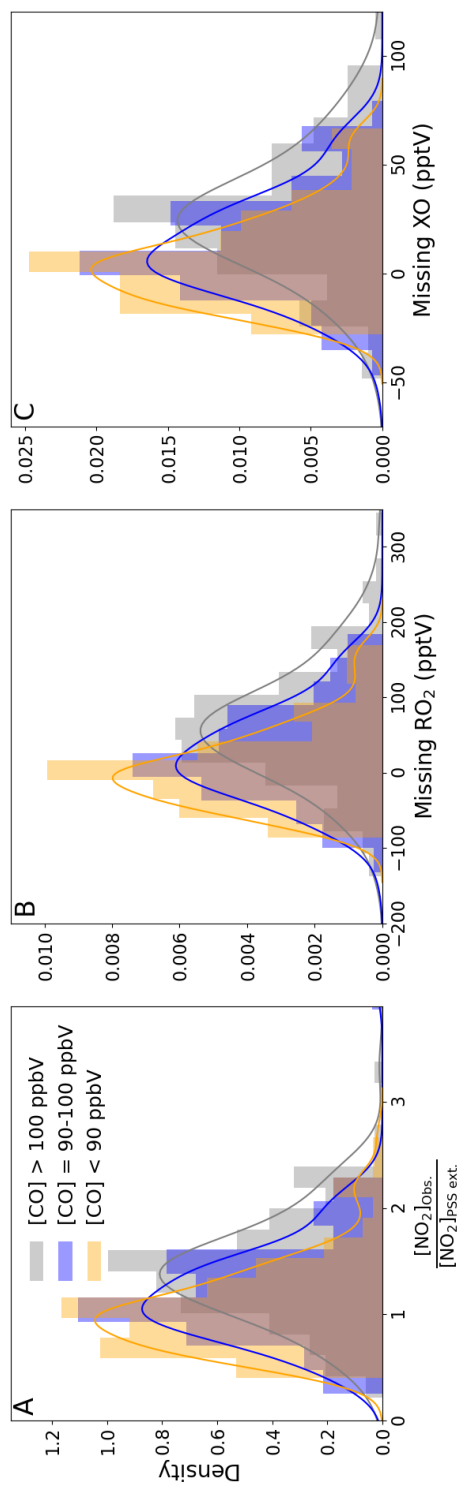
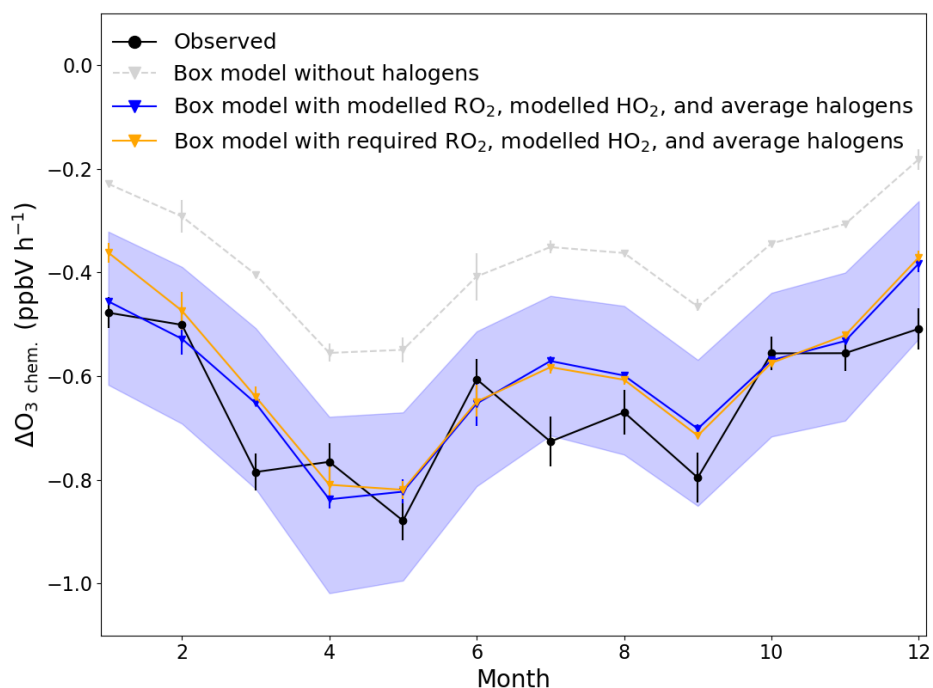


Figure 6: Density distributions of (A) $[\text{NO}_2]_{\text{obs.}}/[\text{NO}_2]_{\text{PSS.ext.}}$, (B) missing RO₂, and (C) missing XO separated by measured CO mixing ratios. An NO₂ artefact of 0.7 pptV has been subtracted from all data.



607

608 Figure 7: Average monthly ΔO_3 due to chemical loss between 09.30 (09.00-10.00) and 17.30
609 (17.00-18.00) UTC for each month (black) compared to box modelled ΔO_3 due to chemical
610 loss using modelled RO_2 and HO_2 with (blue) and without (grey) halogen monoxides (BrO and
611 IO), and using required RO_2 to get $[NO_2]_{Obs.}/[NO_2]_{PSS\ ext.} = 1$, modelled HO_2 , and the annually
612 averaged halogen monoxides (orange). The error bars on the observed chemical loss is the
613 standard error of all the days used for each month and for the box model it is the minimum and
614 maximum ΔO_3 modelled for each month. The blue shaded area show the possible variability
615 in the chemical loss when including the measured halogens at the CVAO (BrO; 2.5 ± 1.1 pptV,
616 IO; 1.4 ± 0.8 pptV) (Read et al., 2008).

617



618 **10 Tables**

619



Table 1: Summary of previous studies which have compared $[RO_x]_{pss}$ against measured and/or modelled $[RO_x]$ in rural, marine and remote conditions.

Location	NO_x instrument	NO_x	ϕ^a	$\frac{[RO_x]_{pss}}{[RO_x]_{measured}}$ ^b	$\frac{[RO_x]_{pss}}{[RO_x]_{model}}$ ^b	$\frac{[RO_x]_{measured}}{[RO_x]_{model}}$ ^b	Reference
Rural conditions							
Hohenpeissenberg, Germany	CLD with PLC ^c	NO; 50-7000 pptV	2-5.7 ^d	2-3 ^e	-	-	(Mannschreck et al., 2004)
Pearl River Delta, China	CLD with PLC ^c	NO; 50-4000 pptV	1-8.5 ^d	~ 1 ^e	2-10	~ 2 ^e	(Ma et al., 2017)
Pabstthum, Germany	CLD with PLC ^c	1-7 ppbV	1.1-3.0 ^d	~ 4 ^e	-	-	(Volz-Thomas et al., 2003)
Idaho Hill, Colorado	CLD with PLC ^c	38 pptV-21.3 ppbV	-	2.1 (mean) ^e	-	~ 1 ^{e,f}	(Cantrell et al., 1997; Williams et al., 1997)
Pine forest, Alabama	CLD with PLC ^c	1-5 ppbV	-	1-2 ^e	-	~ 1 ^{e,f}	(Cantrell et al., 1992; Cantrell et al., 1993a; Parrish et al., 1986)
Essex, England	CLD with Mo ^g	NO; 0.3-9.9 ppbV	-	-	-	~ 1.4 ^e	(Emmerson et al., 2007)
Ponderosa pine forest, Rocky Mountains	CLD with PLC ^c	NO; 100-150 pptV	-	-	-	< 3 ^h	(Wolfe et al., 2014)
Marine/Remote with pollution							
Arabian Peninsula	CLD with PLC ^c and CRDS ⁱ	< 50 pptV - > 10 ppbV	-	-	~ 1	-	(Tadic et al., 2020)
Amazon Basin (Manau)	CLD with PLC ^c	100 pptV - 30 ppbV	1-6 ^d	-	~ 1 ^k	-	(Trebs et al., 2012)
Marine/Remote conditions							
South Atlantic Ocean	CLD with PLC ^c	NO ₂ ; 3-20 pptV	1-12.5 ^l	1.27 ^e	~ 5	~ 4 ^e	(Hosaynali Beygi et al., 2011)
Mauna Loa, Hawaii	CLD with PLC ^c	20-60 pptV	1.4-2.2	1.5-3 ^e	2-3.5	1.2-2 ^e	(Hauglustaine et al., 1996)
Mace Head, Ireland	CLD with TC ^m	NO < 10 pptV	-	-	-	~ 0.25 ^e	(Carpenter et al., 1997; Cox, 1999)
Cape Grim, Tasmania	CLD with PLC ^c	NO < 5 pptV	-	-	-	~ 0.4 ^e	(Carpenter et al., 1997; Cox, 1999)
Cabo Verde	CLD with PLC ^c	< 50 pptV	0.45-12.0 ^d (median = 2.1)	-	1.5 (median)	-	This study



621 ^aWithout radicals and halogens. ^b $[RO_x] = [HO_2] + [RO_2]$. ^cCLD with PLC = Detection by
622 chemiluminescence with photolytic converter for NO_2 . ^dIncreasing ϕ with decreasing $[NO]$,
623 $[NO_2]$ or $[NO_x]$. ^e $[RO_x]$ measured by chemical amplification. ^fCalculated/modelled using stead
624 state theory. ^gCLD with Mo = Detection by chemiluminescence with molybdenum converter.
625 ^h $[RO_x]$ measured by Peroxy Radical Chemical Ionization Mass Spectrometry (PeRCIMS).
626 ⁱCRDS = Cavity Ring down spectroscopy. ^kPSS derived $[RO_x]$ was within the range of the
627 modelled values. ^lIncreasing ϕ with increasing $[NO_2]$. ^mCLD with TC = Detection by
628 chemiluminescence with thermal converter.



629

Table 2: Overview of instruments and measurements used from the CVAO.

Instrument	Measurement	Accuracy	DJF ^a	MAM ^a	JJA ^a	SON ^a	Reference ^b
AQD	NO (pptV)	1.4 pptV	5.3 ± 7.8	1.9 ± 4.2	2.7 ± 5.6	3.6 ± 5.9	Andersen et al. (2021)
	NO ₂ (pptV)	4.4 pptV	27.0 ± 35.8	10.0 ± 13.5	10.2 ± 16.8	10.6 ± 15.7	
Thermo Scientific 49i	O ₃ (ppbV)	0.07 ppbV	38.9 ± 8.8	39.2 ± 12.1	29.9 ± 11.9	31.2 ± 11.1	Read et al. (2008)
Ocean Optics QE650000	<i>j</i> NO ₂ (10 ⁻³ s ⁻¹)	15 %	7.8 ± 2.7	9.3 ± 2.2	8.9 ± 2.5	8.7 ± 2.4	See supplementary
	<i>j</i> O(¹ D) (10 ⁻⁵ s ⁻¹)	15 %	1.7 ± 1.2	3.0 ± 1.3	2.6 ± 1.2	2.6 ± 1.2	Zellweger et al. (2012, 2016)
Picarro	CO (ppbV)	1.0 ppbV	99.0 ± 20.2	103 ± 17	80.0 ± 19.3	84.5 ± 16.6	
	CH ₄ (ppbV)	0.3 ppbV	1916 ± 26	1914 ± 29	1886 ± 34	1896 ± 30	
GC-FID	Ethane (pptV)	5.2 %	1438 ± 600	1204 ± 608	518 ± 267	660 ± 449	
	Ethene (pptV)	5.0 %	31.2 ± 18.6	23.2 ± 9.8	27.5 ± 15.1	28.9 ± 19.6	
	Acetylene (pptV)	10.7 %	134 ± 86	86.9 ± 82.4	22.6 ± 22.2	38.1 ± 38.5	
	Propane (pptV)	5.6 %	336 ± 259	148 ± 195	20.6 ± 18.7	71.0 ± 133	
	Propene (pptV)	6.9 %	8.6 ± 8.6	8.8 ± 11.5	8.0 ± 6.2	7.2 ± 6.1	
	Iso-butane (pptV)	6.4 %	40.4 ± 39.5	11.0 ± 20.0	3.2 ± 4.3	8.4 ± 15.5	R. Steinbrecher (2019)
	n-butane (pptV)	5.0 %	82.8 ± 80.7	19.4 ± 36.0	6.0 ± 7.3	22.1 ± 40.5	
	Iso-pentane (pptV)	4.6 %	11.1 ± 14.9	3.6 ± 6.2	5.2 ± 9.5	4.0 ± 6.7	
	n-pentane (pptV)	6.4 %	8.7 ± 11.4	2.9 ± 4.7	1.7 ± 2.6	3.5 ± 5.2	
	Benzene (pptV)	4.8 %	40.1 ± 30.5	22.9 ± 23.3	11.1 ± 10.5	17.3 ± 11.5	
	Toluene (pptV)	6.3 %	4.6 ± 5.4	3.0 ± 4.2	2.9 ± 2.8	3.4 ± 3.1	
	Methanol (pptV)	20.7 %	486 ± 563	698 ± 734	677 ± 603	857 ± 655	
Acetone (pptV)	12.2 %	506 ± 263	614 ± 274	767 ± 332	681 ± 213		
Campbell Scientific weather station	Temperature (°C)	0.4 °C at 5-40 °C	22.0 ± 2.3	21.7 ± 1.4	24.5 ± 2.5	25.8 ± 2.1	
	Pressure (hPa)	1.0 hPa at 0-40 °C	1016 ± 4	1016 ± 3	1015 ± 4	1014 ± 3	
	Relative Humidity (%)	2 % at 10-90 %	74.9 ± 12.8	77.2 ± 10.4	82.8 ± 8.8	81.1 ± 11.9	Carpenter et al. (2010)
	Solar Radiation (W m ⁻²)	5 %	615 ± 312	785 ± 251	737 ± 283	716 ± 273	

^aMidday (12.00-15.00 UTC, local +1) mean ± 2σ for July 2017 – June 2020. ^bFor further information on the instrument and the data processing.



630
 631

Table 3: Potential sources of NO₂ artefacts at the CVAO.

	ACS at 380 nm (10 ⁻²⁰ cm ⁻²) ^a	ACS at 385 nm (10 ⁻²⁰ cm ⁻²) ^a	ACS at 390 nm (10 ⁻²⁰ cm ⁻²) ^a	Conversion efficiency (%) ^b	Measured at the CVAO at midday (pptV) ^c	Modelled by GEOS Chem at midday (pptV) ^c	Potential artefact (pptV)
$\text{NO}_2 \xrightarrow{h\nu} \text{NO}$	59.24	59.42	62.0	50	-	-	-
$\text{BrONO}_2 \xrightarrow{h\nu} \text{NO}_2$	3.85	3.37	2.97	2.8	-	0.5-1.5	0.014-0.042
$\text{ClONO}_2 \xrightarrow{h\nu} \text{NO}_2$	0.121	0.137	0.091	0.1	-	0.5-1	0.0005-0.001
$\text{ClNO} \xrightarrow{h\nu} \text{NO}$	8.86	7.82	6.86	6.6	-	-	-
$\text{ClNO}_2 \xrightarrow{h\nu} \text{NO}_2$	0.3593	0.2687	0.2008	0.2	-	~0	-
$\text{BrNO}_2 \xrightarrow{h\nu} \text{NO}_2$	17	17	16	14.3	-	~0	-
$\text{HONO} \xrightarrow{h\nu} \text{NO}$	9.2	14.5	2.4	6.3	3-5	0.2-0.4	0.38-0.63
$\text{PAN} \xrightarrow{A} \text{NO}_2$	-	-	-	~5	< 6	~20	< 0.3
Total	-	-	-	-	-	-	0.69-0.97

^aAll absorption cross sections have been reported by IUPAC (Atkinson et al., 2004). ^bThe reported conversion efficiencies have been calculated based on a NO₂ CE of 50%. ^cMidday is defined as 12:00-15:00 UTC (local+1).



632

Table 4: Summary over the required additional artefact, RO₂, and XO to give [NO₂]_{obs./[NO₂]_{pSS ext. = 1 given as 50th (25th-75th) percentile when subtracting a NO₂ artefact of 0.7 pptV.}}

	[CO] < 90 ppbV	90 ppbV < [CO] < 100 ppbV	[CO] > 100 ppbV
$\frac{[\text{NO}_2]_{\text{obs.}}}{[\text{NO}_2]_{\text{pSS ext.}}}$	1.00 (0.76 - 1.29)	1.14 (0.89 - 1.47)	1.42 (1.12 - 1.68)
Required additional artefact (pptV)	0.00 (-2.65 - 1.70)	1.9 (0.92 - 5.27)	4.4 (0.95 - 9.27)
Case I: Using BrO = 2.5 pptV and IO = 1.4 pptV			
Required RO _x (pptV) ^a	49.45 (16.18 - 87.63)	65.0 (33.68 - 112.5)	109.7 (63.14 - 149.5)
Modelled RO _x (pptV)	48.89 (46.01 - 53.35)	45.60 (35.69 - 54.71)	44.99 (37.31 - 54.70)
Required RO ₂ (pptV) ^b	31.77 (-1.79 - 69.99)	47.53 (16.81 - 93.93)	90.49 (45.04 - 128.5)
Modelled RO ₂ (pptV)	33.66 (30.07 - 34.43)	29.89 (21.50 - 36.32)	27.62 (20.93 - 35.42)
Missing RO ₂ (pptV) ^c	-0.25 (-31.85 - 39.69)	20.19 (-14.23 - 66.44)	61.33 (18.53 - 104.3)
Case II: Using modelled RO₂ and HO₂			
Required XO (pptV) ^d	3.72 (-7.94 - 18.55)	11.31 (-1.46 - 28.46)	26.58 (10.70 - 42.52)
Missing XO (pptV) ^e	-0.18 (-11.84 - 14.65)	7.41 (-5.36 - 24.56)	22.68 (6.80 - 38.62)

^aCalculated using equation (IV). ^bCalculated using equation (VIII). ^cCalculated using equation (IX). ^dCalculated using equation (V).

^eSubtracted 3.9 pptV of XO from the required XO (2.5 pptV BrO + 1.4 pptV IO).



11 References

- 635 Andersen, S. T., Carpenter, L. J., Nelson, B. S., Neves, L., Read, K. A., Reed, C., Ward, M.,
Rowlinson, M. J., and Lee, J. D.: Long-term NO_x measurements in the remote marine
tropical troposphere, *Atmos. Meas. Tech.*, 14, 3071-3085, 10.5194/amt-14-3071-2021,
2021.
- Atkinson, R., Baulch, D. L., Cox, R. A., Crowley, J. N., Hampson, R. F., Hynes, R. G., Jenkin,
M. E., Rossi, M. J., and Troe, J.: IUPAC Task Group on Atmospheric Chemical Kinetic
640 Data Evaluation, *Atmos. Chem. Phys.*, 4, 2004.
- Atkinson, R., Baulch, D. L., Cox, R. A., Crowley, J. N., Hampson, R. F., Hynes, R. G., Jenkin,
M. E., Rossi, M. J., Troe, J., and Subcommittee, I.: Evaluated kinetic and photochemical
data for atmospheric chemistry: Volume II – gas phase reactions of organic species,
Atmos. Chem. Phys., 6, 3625-4055, 10.5194/acp-6-3625-2006, 2006.
- 645 Ayers, G. P., Penkett, S. A., Gillett, R. W., Bandy, B., Galbally, I. E., Meyer, C. P., Elsworth,
C. M., Bentley, S. T., and Forgan, B. W.: Evidence for photochemical control of ozone
concentrations in unpolluted marine air, *Nature*, 360, 446-449, 10.1038/360446a0, 1992.
- Ayers, G. P., and Galbally, I. E.: A preliminary investigation of a boundary layer-free
troposphere entrainment velocity at Cape Grim, *Baseline* 92, 1995.
- 650 Bloss, W. J., Evans, M. J., Lee, J. D., Sommariva, R., Heard, D. E., and Pilling, M. J.: The
oxidative capacity of the troposphere: Coupling of field measurements of OH and a global
chemistry transport model, *Faraday Discussions*, 130, 425-436, 10.1039/B419090D, 2005.
- Bradshaw, J., Davis, D., Crawford, J., Chen, G., Shetter, R., Müller, M., Gregory, G., Sachse,
G., Blake, D., Heikes, B., Singh, H., Mastromarino, J., and Sandholm, S.:
655 Photofragmentation two-photon laser-induced fluorescence detection of NO₂ and NO:
Comparison of measurements with model results based on airborne observations during
PEM-Tropics A, *Geophysical Research Letters*, 26, 471-474,
<https://doi.org/10.1029/1999GL900015>, 1999.
- Bridier, I., Caralp, F., Loirat, H., Lesclaux, R., Veyret, B., Becker, K. H., Reimer, A., and
660 Zabel, F.: Kinetic and theoretical studies of the reactions acetylperoxy + nitrogen dioxide
+ M. dblarw. acetyl peroxy + M between 248 and 393 K and between 30 and 760
torr, *The Journal of Physical Chemistry*, 95, 3594-3600, 10.1021/j100162a031, 1991.
- Burkert, J., Andrés-Hernández, M.-D., Stöbener, D., Burrows, J. P., Weissenmayer, M., and
Kraus, A.: Peroxy radical and related trace gas measurements in the boundary layer above
665 the Atlantic Ocean, *Journal of Geophysical Research: Atmospheres*, 106, 5457-5477,
<https://doi.org/10.1029/2000JD900613>, 2001.
- Butkovskaya, N., Kukui, A., and Le Bras, G.: HNO₃ Forming Channel of the HO₂ + NO
Reaction as a Function of Pressure and Temperature in the Ranges of 72–600 Torr and
223–323 K, *The Journal of Physical Chemistry A*, 111, 9047-9053, 10.1021/jp074117m,
670 2007.
- Butkovskaya, N., Rayez, M.-T., Rayez, J.-C., Kukui, A., and Le Bras, G.: Water Vapor Effect
on the HNO₃ Yield in the HO₂ + NO Reaction: Experimental and Theoretical Evidence,
The Journal of Physical Chemistry A, 113, 11327-11342, 10.1021/jp811428p, 2009.
- Calvert, J. G., and Stockwell, W. R.: Deviations from the O₃-NO-NO₂ photostationary state
675 in tropospheric chemistry, *Canadian Journal of Chemistry*, 61, 983-992, 10.1139/v83-174,
1983.
- Cantrell, C. A., Lind, J. A., Shetter, R. E., Calvert, J. G., Goldan, P. D., Kuster, W., Fehsenfeld,
F. C., Montzka, S. A., Parrish, D. D., Williams, E. J., Buhr, M. P., Westberg, H. H.,
Allwine, G., and Martin, R.: Peroxy radicals in the ROSE experiment: Measurement and
680 theory, *Journal of Geophysical Research: Atmospheres*, 97, 20671-20686,
<https://doi.org/10.1029/92JD01727>, 1992.



- 685 Cantrell, C. A., Shetter, R. E., Calvert, J. G., Parrish, D. D., Fehsenfeld, F. C., Goldan, P. D.,
Kuster, W., Williams, E. J., Westberg, H. H., Allwine, G., and Martin, R.: Peroxy radicals
as measured in ROSE and estimated from photostationary state deviations, *Journal of*
Geophysical Research: Atmospheres, 98, 18355-18366,
<https://doi.org/10.1029/93JD01794>, 1993a.
- 690 Cantrell, C. A., Shetter, R. E., Lind, J. A., McDaniel, A. H., Calvert, J. G., Parrish, D. D.,
Fehsenfeld, F. C., Buhr, M. P., and Trainer, M.: An improved chemical amplifier technique
for peroxy radical measurements, *Journal of Geophysical Research: Atmospheres*, 98,
2897-2909, <https://doi.org/10.1029/92JD02842>, 1993b.
- Cantrell, C. A., Shetter, R. E., Gilpin, T. M., and Calvert, J. G.: Peroxy radicals measured
during Mauna Loa Observatory Photochemistry Experiment 2: The data and first analysis,
Journal of Geophysical Research: Atmospheres, 101, 14643-14652,
<https://doi.org/10.1029/95JD01698>, 1996.
- 695 Cantrell, C. A., Shetter, R. E., Calvert, J. G., Eisele, F. L., Williams, E., Baumann, K., Brune,
W. H., Stevens, P. S., and Mather, J. H.: Peroxy radicals from photostationary state
deviations and steady state calculations during the Tropospheric OH Photochemistry
Experiment at Idaho Hill, Colorado, 1993, *Journal of Geophysical Research: Atmospheres*,
102, 6369-6378, <https://doi.org/10.1029/96JD01703>, 1997.
- 700 Carpenter, L. J., Monks, P. S., Bandy, B. J., Penkett, S. A., Galbally, I. E., and Meyer, C. P.: A
study of peroxy radicals and ozone photochemistry at coastal sites in the northern and
southern hemispheres, *Journal of Geophysical Research: Atmospheres*, 102, 25417-25427,
<https://doi.org/10.1029/97JD02242>, 1997.
- 705 Carpenter, L. J., Clemmitshaw, K. C., Burgess, R. A., Penkett, S. A., Cape, J. N., and McFadyen,
G. G.: Investigation and evaluation of the NO_x/O₃ photochemical steady state,
Atmospheric Environment, 32, 3353-3365, [https://doi.org/10.1016/S1352-
2310\(97\)00416-0](https://doi.org/10.1016/S1352-2310(97)00416-0), 1998.
- 710 Carpenter, L. J., Fleming, Z. L., Read, K. A., Lee, J. D., Moller, S. J., Hopkins, J. R., Purvis,
R. M., Lewis, A. C., Müller, K., Heinold, B., Herrmann, H., Fomba, K. W., van Pinxteren,
D., Müller, C., Tegen, I., Wiedensohler, A., Müller, T., Niedermeier, N., Achterberg, E.
P., Patey, M. D., Kozlova, E. A., Heimann, M., Heard, D. E., Plane, J. M. C., Mahajan, A.,
Oetjen, H., Ingham, T., Stone, D., Whalley, L. K., Evans, M. J., Pilling, M. J., Leigh, R.
J., Monks, P. S., Karunaharan, A., Vaughan, S., Arnold, S. R., Tschritter, J., Pöhler, D.,
Frieß, U., Holla, R., Mendes, L. M., Lopez, H., Faria, B., Manning, A. J., and Wallace, D.
715 W. R.: Seasonal characteristics of tropical marine boundary layer air measured at the Cape
Verde Atmospheric Observatory, *Journal of Atmospheric Chemistry*, 67, 87-140,
[10.1007/s10874-011-9206-1](https://doi.org/10.1007/s10874-011-9206-1), 2010.
- Carsey, T. P., Churchill, D. D., Farmer, M. L., Fischer, C. J., Pszenny, A. A., Ross, V. B.,
Saltzman, E. S., Springer-Young, M., and Bonsang, B.: Nitrogen oxides and ozone
720 production in the North Atlantic marine boundary layer, *Journal of Geophysical Research:*
Atmospheres, 102, 10653-10665, [10.1029/96JD03511](https://doi.org/10.1029/96JD03511), 1997.
- Clemmitshaw, K. C., Carpenter, L. J., Penkett, S. A., and Jenkin, M. E.: A calibrated peroxy
radical chemical amplifier for ground-based tropospheric measurements, *Journal of*
Geophysical Research: Atmospheres, 102, 25405-25416,
725 <https://doi.org/10.1029/97JD01902>, 1997.
- Cox, R. A.: Ozone and peroxy radical budgets in the marine boundary layer: Modeling the
effect of NO_x, *Journal of Geophysical Research: Atmospheres*, 104, 8047-8056,
<https://doi.org/10.1029/1998JD100104>, 1999.
- 730 Crawford, J., Davis, D., Chen, G., Bradshaw, J., Sandholm, S., Gregory, G., Sachse, G.,
Anderson, B., Collins, J., Blake, D., Singh, H., Heikes, B., Talbot, R., and Rodriguez, J.:
Photostationary state analysis of the NO₂-NO system based on airborne observations from



- the western and central North Pacific, *Journal of Geophysical Research: Atmospheres*, 101, 2053-2072, <https://doi.org/10.1029/95JD02201>, 1996.
- 735 Duncianu, M., Lahib, A., Tomas, A., Stevens, P. S., and Dusanter, S.: Characterization of a chemical amplifier for peroxy radical measurements in the atmosphere, *Atmospheric Environment*, 222, 117106, <https://doi.org/10.1016/j.atmosenv.2019.117106>, 2020.
- Emmerson, K. M., Carslaw, N., Carslaw, D. C., Lee, J. D., McFiggans, G., Bloss, W. J., Gravestock, T., Heard, D. E., Hopkins, J., Ingham, T., Pilling, M. J., Smith, S. C., Jacob, M., and Monks, P. S.: Free radical modelling studies during the UK TORCH Campaign in
740 Summer 2003, *Atmos. Chem. Phys.*, 7, 167-181, 10.5194/acp-7-167-2007, 2007.
- Fairlie, T. D., Jacob, D. J., Dibb, J. E., Alexander, B., Avery, M. A., van Donkelaar, A., and Zhang, L.: Impact of mineral dust on nitrate, sulfate, and ozone in transpacific Asian pollution plumes, *Atmos. Chem. Phys.*, 10, 3999-4012, 10.5194/acp-10-3999-2010, 2010.
- 745 Gao, R. S., Keim, E. R., Woodbridge, E. L., Ciciora, S. J., Proffitt, M. H., Thompson, T. L., Mclaughlin, R. J., and Fahey, D. W.: New photolysis system for NO₂ measurements in the lower stratosphere, *Journal of Geophysical Research: Atmospheres*, 99, 20673-20681, <https://doi.org/10.1029/94JD01521>, 1994.
- Handisides, G. M., Plass-Dülmer, C., Gilge, S., Bingemer, H., and Berresheim, H.: Hohenpeissenberg Photochemical Experiment (HOPE 2000): Measurements and photostationary state calculations of OH and peroxy radicals, *Atmos. Chem. Phys.*, 3, 1565-1588, 10.5194/acp-3-1565-2003, 2003.
- 750 Hauglustaine, D. A., Madronich, S., Ridley, B. A., Walega, J. G., Cantrell, C. A., Shetter, R. E., and Hübler, G.: Observed and model-calculated photostationary state at Mauna Loa Observatory during MLOPEX 2, *Journal of Geophysical Research: Atmospheres*, 101, 14681-14696, <https://doi.org/10.1029/95JD03612>, 1996.
- 755 Hauglustaine, D. A., Madronich, S., Ridley, B. A., Flocke, S. J., Cantrell, C. A., Eisele, F. L., Shetter, R. E., Tanner, D. J., Ginoux, P., and Atlas, E. L.: Photochemistry and budget of ozone during the Mauna Loa Observatory Photochemistry Experiment (MLOPEX 2), *Journal of Geophysical Research: Atmospheres*, 104, 30275-30307, <https://doi.org/10.1029/1999JD900441>, 1999.
- 760 Hernández, M. D. A., Burkert, J., Reichert, L., Stöbener, D., Meyer-Arne, J., Burrows, J. P., Dickerson, R. R., and Doddridge, B. G.: Marine boundary layer peroxy radical chemistry during the AEROSOLS99 campaign: Measurements and analysis, *Journal of Geophysical Research: Atmospheres*, 106, 20833-20846, <https://doi.org/10.1029/2001JD900113>, 2001.
- 765 Hosaynali Beygi, Z., Fischer, H., Harder, H. D., Martinez, M., Sander, R., Williams, J., Brookes, D. M., Monks, P. S., and Lelieveld, J.: Oxidation photochemistry in the Southern Atlantic boundary layer: unexpected deviations of photochemical steady state, *Atmos. Chem. Phys.*, 11, 8497-8513, 10.5194/acp-11-8497-2011, 2011.
- 770 Inamdar, S., Tinel, L., Chance, R., Carpenter, L. J., Sabu, P., Chacko, R., Tripathy, S. C., Kerkar, A. U., Sinha, A. K., Bhaskar, P. V., Sarkar, A., Roy, R., Sherwen, T., Cuevas, C., Saiz-Lopez, A., Ram, K., and Mahajan, A. S.: Estimation of reactive inorganic iodine fluxes in the Indian and Southern Ocean marine boundary layer, *Atmos. Chem. Phys.*, 20, 12093-12114, 10.5194/acp-20-12093-2020, 2020.
- 775 Jacob, D. J., Heikes, E. G., Fan, S.-M., Logan, J. A., Mauzerall, D. L., Bradshaw, J. D., Singh, H. B., Gregory, G. L., Talbot, R. W., Blake, D. R., and Sachse, G. W.: Origin of ozone and NO_x in the tropical troposphere: A photochemical analysis of aircraft observations over the South Atlantic basin, 101, 24235-24250, doi:10.1029/96JD00336, 1996.
- Jenkin, M. E., Young, J. C., and Rickard, A. R.: The MCM v3.3.1 degradation scheme for isoprene, *Atmos. Chem. Phys.*, 15, 11433-11459, 10.5194/acp-15-11433-2015, 2015.
- 780 Kleindienst, T. E.: Recent developments in the chemistry and biology of peroxyacetyl nitrate, *Research on Chemical Intermediates*, 20, 335-384, 10.1163/156856794X00379, 1994.



- 785 Lee, J. D., Moller, S. J., Read, K. A., Lewis, A. C., Mendes, L., and Carpenter, L. J.: Year-round measurements of nitrogen oxides and ozone in the tropical North Atlantic marine boundary layer, *Journal of Geophysical Research: Atmospheres*, 114, <https://doi.org/10.1029/2009JD011878>, 2009.
- Leighton, P. A.: *Photochemistry of Air Pollution*, Academic Press, 1961.
- Liu, Y., and Zhang, J.: Atmospheric Peroxy Radical Measurements Using Dual-Channel Chemical Amplification Cavity Ringdown Spectroscopy, *Analytical chemistry*, 86, 5391-5398, [10.1021/ac5004689](https://doi.org/10.1021/ac5004689), 2014.
- 790 Ma, Y., Lu, K., Chou, C. C. K., Li, X., and Zhang, Y.: Strong deviations from the NO-NO₂-O₃ photostationary state in the Pearl River Delta: Indications of active peroxy radical and chlorine radical chemistry, *Atmospheric Environment*, 163, 22-34, <https://doi.org/10.1016/j.atmosenv.2017.05.012>, 2017.
- 795 Mahajan, A. S., Plane, J. M. C., Oetjen, H., Mendes, L., Saunders, R. W., Saiz-Lopez, A., Jones, C. E., Carpenter, L. J., and McFiggans, G. B.: Measurement and modelling of tropospheric reactive halogen species over the tropical Atlantic Ocean, *Atmos. Chem. Phys.*, 10, 4611-4624, [10.5194/acp-10-4611-2010](https://doi.org/10.5194/acp-10-4611-2010), 2010.
- 800 Mannschreck, K., Gilge, S., Plass-Duelmer, C., Fricke, W., and Berresheim, H.: Assessment of the applicability of NO-NO₂-O₃ photostationary state to long-term measurements at the Hohenpeissenberg GAW Station, Germany, *Atmos. Chem. Phys.*, 4, 1265-1277, [10.5194/acp-4-1265-2004](https://doi.org/10.5194/acp-4-1265-2004), 2004.
- Mihele, C. M., and Hastie, D. R.: The sensitivity of the radical amplifier to ambient water vapour, *Geophysical Research Letters*, 25, 1911-1913, <https://doi.org/10.1029/98GL01432>, 1998.
- 805 Miyazaki, K., Parker, A. E., Fittschen, C., Monks, P. S., and Kajii, Y.: A new technique for the selective measurement of atmospheric peroxy radical concentrations of HO₂ and RO₂ using a denuding method, *Atmos. Meas. Tech.*, 3, 1547-1554, [10.5194/amt-3-1547-2010](https://doi.org/10.5194/amt-3-1547-2010), 2010.
- 810 Parrish, D. D., Trainer, M., Williams, E. J., Fahey, D. W., Hübler, G., Eubank, C. S., Liu, S. C., Murphy, P. C., Albritton, D. L., and Fehsenfeld, F. C.: Measurements of the NO_x-O₃ photostationary state at Niwot Ridge, Colorado, *Journal of Geophysical Research: Atmospheres*, 91, 5361-5370, <https://doi.org/10.1029/JD091iD05p05361>, 1986.
- 815 Parrish, D. D., Hahn, C. H., Fahey, D. W., Williams, E. J., Bollinger, M. J., Hübler, G., Buhr, M. P., Murphy, P. C., Trainer, M., Hsie, E. Y., Liu, S. C., and Fehsenfeld, F. C.: Systematic variations in the concentration of NO_x (NO Plus NO₂) at Niwot Ridge, Colorado, *Journal of Geophysical Research: Atmospheres*, 95, 1817-1836, <https://doi.org/10.1029/JD095iD02p01817>, 1990.
- Peterson, M. C., and Honrath, R. E.: NO_x and NO_y over the northwestern North Atlantic: Measurements and measurement accuracy, *Journal of Geophysical Research: Atmospheres*, 104, 11695-11707, 1999.
- 820 Pinto, J. P., Dibb, J., Lee, B. H., Rappenglück, B., Wood, E. C., Levy, M., Zhang, R.-Y., Lefer, B., Ren, X.-R., Stutz, J., Tsai, C., Ackermann, L., Golovko, J., Herndon, S. C., Oakes, M., Meng, Q.-Y., Munger, J. W., Zahniser, M., and Zheng, J.: Intercomparison of field measurements of nitrous acid (HONO) during the SHARP campaign, *Journal of Geophysical Research: Atmospheres*, 119, 5583-5601, <https://doi.org/10.1002/2013JD020287>, 2014.
- 825 Pollack, I. B., Lerner, B. M., and Ryerson, T. B.: Evaluation of ultraviolet light-emitting diodes for detection of atmospheric NO₂ by photolysis - chemiluminescence, *Journal of Atmospheric Chemistry*, 65, 111-125, [10.1007/s10874-011-9184-3](https://doi.org/10.1007/s10874-011-9184-3), 2010.
- 830 Prados-Roman, C., Cuevas, C. A., Hay, T., Fernandez, R. P., Mahajan, A. S., Royer, S. J., Galí, M., Simó, R., Dachs, J., Großmann, K., Kinnison, D. E., Lamarque, J. F., and Saiz-Lopez,



- A.: Iodine oxide in the global marine boundary layer, *Atmos. Chem. Phys.*, 15, 583-593, 10.5194/acp-15-583-2015, 2015.
- 835 Read, K. A., Mahajan, A. S., Carpenter, L. J., Evans, M. J., Faria, B. V. E., Heard, D. E., Hopkins, J. R., Lee, J. D., Moller, S. J., Lewis, A. C., Mendes, L., McQuaid, J. B., Oetjen, H., Saiz-Lopez, A., Pilling, M. J., and Plane, J. M. C.: Extensive halogen-mediated ozone destruction over the tropical Atlantic Ocean, *Nature*, 453, 1232, 10.1038/nature07035
- <https://www.nature.com/articles/nature07035#supplementary-information>, 2008.
- 840 Read, K. A., Lee, J. D., Lewis, A. C., Moller, S. J., Mendes, L., and Carpenter, L. J.: Intra-annual cycles of NMVOC in the tropical marine boundary layer and their use for interpreting seasonal variability in CO, *Journal of Geophysical Research: Atmospheres*, 114, <https://doi.org/10.1029/2009JD011879>, 2009.
- 845 Reed, C., Evans, M. J., Carlo, P. D., Lee, J. D., and Carpenter, L. J.: Interferences in photolytic NO₂ measurements: explanation for an apparent missing oxidant?, *Atmospheric Chemistry Physics*, 16, 4707-4724, 2016.
- Reed, C., Evans, M. J., Crilley, L. R., Bloss, W. J., Sherwen, T., Read, K. A., Lee, J. D., and Carpenter, L. J.: Evidence for renoxification in the tropical marine boundary layer, *Atmos. Chem. Phys.*, 17, 4081-4092, 10.5194/acp-17-4081-2017, 2017.
- 850 Rhoads, K. P., Kelley, P., Dickerson, R. R., Carsey, T. P., Farmer, M., Savoie, D. L., and Prospero, J. M.: Composition of the troposphere over the Indian Ocean during the monsoonal transition, *Journal of Geophysical Research: Atmospheres*, 102, 18981-18995, 10.1029/97JD01078, 1997.
- 855 Ridley, B. A., Carroll, M. A., Gregory, G. L., and Sachse, G. W.: NO and NO₂ in the troposphere: Technique and measurements in regions of a folded tropopause, *Journal of Geophysical Research: Atmospheres*, 93, 15813-15830, <https://doi.org/10.1029/JD093iD12p15813>, 1988.
- Ridley, B. A., Madronich, S., Chatfield, R. B., Walega, J. G., Shetter, R. E., Carroll, M. A., and Montzka, D. D.: Measurements and model simulations of the photostationary state during the Mauna Loa Observatory Photochemistry Experiment: Implications for radical concentrations and ozone production and loss rates, *Journal of Geophysical Research: Atmospheres*, 97, 10375-10388, <https://doi.org/10.1029/91JD02287>, 1992.
- Ryerson, T. B., Williams, E. J., and Fehsenfeld, F. C.: An efficient photolysis system for fast-response NO₂ measurements, *Journal of Geophysical Research: Atmospheres*, 105, 26447-26461, 10.1029/2000jd900389, 2000.
- 865 Sadanaga, Y., Matsumoto, J., Sakurai, K.-i., Isozaki, R., Kato, S., Nomaguchi, T., Bandow, H., and Kajii, Y.: Development of a measurement system of peroxy radicals using a chemical amplification/laser-induced fluorescence technique, *Review of Scientific Instruments*, 75, 864-872, 10.1063/1.1666985, 2004.
- 870 Saiz-Lopez, A., Plane, J. M. C., Baker, A. R., Carpenter, L. J., von Glasow, R., Gómez Martín, J. C., McFiggans, G., and Saunders, R. W.: Atmospheric Chemistry of Iodine, *Chemical Reviews*, 112, 1773-1804, 10.1021/cr200029u, 2012.
- Sherwen, T., Evans, M. J., Carpenter, L. J., Andrews, S. J., Lidster, R. T., Dix, B., Koenig, T. K., Sinreich, R., Ortega, I., Volkamer, R., Saiz-Lopez, A., Prados-Roman, C., Mahajan, A. S., and Ordóñez, C.: Iodine's impact on tropospheric oxidants: a global model study in GEOS-Chem, *Atmos. Chem. Phys.*, 16, 1161-1186, 10.5194/acp-16-1161-2016, 2016.
- 875 Sillman, S.: The relation between ozone, NO_x and hydrocarbons in urban and polluted rural environments, *Atmospheric Environment*, 33, 1821-1845, [https://doi.org/10.1016/S1352-2310\(98\)00345-8](https://doi.org/10.1016/S1352-2310(98)00345-8), 1999.
- 880 Sommariva, R., Cox, S., Martin, C., Borońska, K., Young, J., Jimack, P. K., Pilling, M. J., Matthaios, V. N., Nelson, B. S., Newland, M. J., Panagi, M., Bloss, W. J., Monks, P. S.,



- and Rickard, A. R.: AtChem (version 1), an open-source box model for the Master Chemical Mechanism, *Geosci. Model Dev.*, 13, 169-183, 10.5194/gmd-13-169-2020, 2020.
- 885 Steinbrecher, R.: SYSTEM AND PERFORMANCE AUDIT FOR NON METHANE VOLATILE ORGANIC COMPOUNDS: Global GAW Station – Cape Verde Atmospheric Observatory Calhau, Cape Verde, WMO World Calibration Centre for VOC, Karlsruhe Institute of Technology, KIT/IMK-IFU, Garmisch-Partenkirchen, Germany, 2019.
- 890 Tadic, I., Crowley, J. N., Dienhart, D., Eger, P., Harder, H., Hottmann, B., Martinez, M., Parchatka, U., Paris, J. D., Pozzer, A., Rohloff, R., Schuladen, J., Shenolikar, J., Tauer, S., Lelieveld, J., and Fischer, H.: Net ozone production and its relationship to nitrogen oxides and volatile organic compounds in the marine boundary layer around the Arabian Peninsula, *Atmos. Chem. Phys.*, 20, 6769-6787, 10.5194/acp-20-6769-2020, 2020.
- 895 Trebs, I., Mayol-Bracero, O. L., Pauliquevis, T., Kuhn, U., Sander, R., Ganzeveld, L., Meixner, F. X., Kesselmeier, J., Artaxo, P., and Andreae, M. O.: Impact of the Manaus urban plume on trace gas mixing ratios near the surface in the Amazon Basin: Implications for the NO-NO₂-O₃ photostationary state and peroxy radical levels, *Journal of Geophysical Research: Atmospheres*, 117, <https://doi.org/10.1029/2011JD016386>, 2012.
- 900 Vaughan, S., Ingham, T., Whalley, L. K., Stone, D., Evans, M. J., Read, K. A., Lee, J. D., Moller, S. J., Carpenter, L. J., Lewis, A. C., Fleming, Z. L., and Heard, D. E.: Seasonal observations of OH and HO₂ in the remote tropical marine boundary layer, *Atmos. Chem. Phys.*, 12, 2149-2172, 10.5194/acp-12-2149-2012, 2012.
- 905 Vogt, R., Sander, R., von Glasow, R., and Crutzen, P. J.: Iodine Chemistry and its Role in Halogen Activation and Ozone Loss in the Marine Boundary Layer: A Model Study, *Journal of Atmospheric Chemistry*, 32, 375-395, 10.1023/A:1006179901037, 1999.
- 910 Volz-Thomas, A., Pätz, H.-W., Houben, N., Konrad, S., Mihelcic, D., Klüpfel, T., and Perner, D.: Inorganic trace gases and peroxy radicals during BERLIOZ at Pabstthum: An investigation of the photostationary state of NO_x and O₃, *Journal of Geophysical Research: Atmospheres*, 108, PHO 4-1-PHO 4-15, <https://doi.org/10.1029/2001JD001255>, 2003.
- 915 Wang, X., Jacob, D. J., Downs, W., Zhai, S., Zhu, L., Shah, V., Holmes, C. D., Sherwen, T., Alexander, B., Evans, M. J., Eastham, S. D., Neuman, J. A., Veres, P. R., Koenig, T. K., Volkamer, R., Huey, L. G., Bannan, T. J., Percival, C. J., Lee, B. H., and Thornton, J. A.: Global tropospheric halogen (Cl, Br, I) chemistry and its impact on oxidants, *Atmos. Chem. Phys.*, 21, 13973-13996, 10.5194/acp-21-13973-2021, 2021.
- 920 Whalley, L. K., Lewis, A. C., McQuaid, J. B., Purvis, R. M., Lee, J. D., Stemmler, K., Zellweger, C., and Ridgeon, P.: Two high-speed, portable GC systems designed for the measurement of non-methane hydrocarbons and PAN: Results from the Jungfraujoch High Altitude Observatory, *Journal of Environmental Monitoring*, 6, 234-241, 10.1039/B310022G, 2004.
- 925 Whalley, L. K., Furneaux, K. L., Goddard, A., Lee, J. D., Mahajan, A., Oetjen, H., Read, K. A., Kaaden, N., Carpenter, L. J., Lewis, A. C., Plane, J. M. C., Saltzman, E. S., Wiedensohler, A., and Heard, D. E.: The chemistry of OH and HO₂ radicals in the boundary layer over the tropical Atlantic Ocean, *Atmos. Chem. Phys.*, 10, 1555-1576, 10.5194/acp-10-1555-2010, 2010.
- Williams, E. J., Roberts, J. M., Baumann, K., Bertman, S. B., Buhr, S., Norton, R. B., and Fehsenfeld, F. C.: Variations in NO_y composition at Idaho Hill, Colorado, *Journal of Geophysical Research: Atmospheres*, 102, 6297-6314, <https://doi.org/10.1029/96JD03252>, 1997.



- 930 Wolfe, G. M., Cantrell, C., Kim, S., Mauldin Iii, R. L., Karl, T., Harley, P., Turnipseed, A.,
Zheng, W., Flocke, F., Apel, E. C., Hornbrook, R. S., Hall, S. R., Ullmann, K., Henry, S.
B., DiGangi, J. P., Boyle, E. S., Kaser, L., Schnitzhofer, R., Hansel, A., Graus, M.,
Nakashima, Y., Kajii, Y., Guenther, A., and Keutsch, F. N.: Missing peroxy radical sources
within a summertime ponderosa pine forest, *Atmos. Chem. Phys.*, 14, 4715-4732,
935 10.5194/acp-14-4715-2014, 2014.
- Wood, E. C., and Charest, J. R.: Chemical Amplification - Cavity Attenuated Phase Shift
Spectroscopy Measurements of Atmospheric Peroxy Radicals, *Analytical chemistry*, 86,
10266-10273, 10.1021/ac502451m, 2014.
- 940 Zellweger, C., Steinbacher, M., and Buchmann, B.: Evaluation of new laser spectrometer
techniques for in-situ carbon monoxide measurements, *Atmos. Meas. Tech.*, 5, 2555-2567,
10.5194/amt-5-2555-2012, 2012.
- Zellweger, C., Emmenegger, L., Firdaus, M., Hatakka, J., Heimann, M., Kozlova, E., Spain, T.
G., Steinbacher, M., van der Schoot, M. V., and Buchmann, B.: Assessment of recent
advances in measurement techniques for atmospheric carbon dioxide and methane
945 observations, *Atmos. Meas. Tech.*, 9, 4737-4757, 10.5194/amt-9-4737-2016, 2016.